NAVAL POSTGRADUATE SCHOOL
MONTEREY, CALIFORNIA

THESIS

EQUIVALENT IMPEDANCE OF ROUGH SURFACE AT LOW GRAZING ANGLES

by

Marcelo Jorge de Assis Motta

September 1999

Thesis Advisor: Ramakrishna Janaswamy
Second Reader: David Jenn

Approved for public release; distribution is unlimited.

REPORT DOCUMENTATION PAGE

Form Approved OMB No. 0704-0188.

1. AGENCY USE ONLY *(Leave blank)*	2. REPORT DATE	3. REPORT TYPE AND DATES COVERED
	September 1999	Master's Thesis

4. TITLE AND SUBTITLE
EQUIVALENT IMPEDANCE OF ROUGH SURFACE AT LOW GRAZING ANGLES

5. FUNDING NUMBERS

6. AUTHOR(S)
Marcelo Jorge de Assis Motta

7. PERFORMING ORGANIZATION NAME(S) AND ADDRESS(ES)
Naval Postgraduate School
Monterey, CA 93943-5000

8. PERFORMING ORGANIZATION REPORT NUMBER

9. SPONSORING/MONITORING AGENCY NAME(S) AND ADDRESS(ES)

10. SPONSORING / MONITORING AGENCY REPORT NUMBER

11. SUPPLEMENTARY NOTES
The views expressed in this thesis are those of the author and do not reflect the official policy or position of the Department of Defense or the U.S. Government.

12a. DISTRIBUTION / AVAILABILITY STATEMENT
Approved for public release; distribution is unlimited.

12b. DISTRIBUTION CODE

13. ABSTRACT *(maximum 200 words)*

Equivalent impedance of a rough surface is determined by solving the problem of radiowave propagation over rough random surface by using the parabolic equation method. We consider horizontal polarization and assume the rough surface, defined by discrete points, to be perfectly conducting. This assumption has minimum effects for frequencies in the VHF band and above. The essential point of this thesis is to solve numerically a Volterra integral equation of the second kind for the surface current. Because the computation becomes very intense for long ranges, we present a multiple sections solution, where the solution procedure is successively repeated for smaller ranges. The numerical results are compared with results available in the literature. Finally, we apply the technique to determine the equivalent impedance of a sinusoidal random rough surface by comparing the resulting normalized field to the field of a 2-ray model over a constant impedance plane.

14. SUBJECT TERMS
Radiowave Propagation, Volterra Integral Equation, Low Grazing Angle, Propagation on Rough Random Surface, Equivalent Impedance Determination

15. NUMBER OF PAGES
91

16. PRICE CODE

17. SECURITY CLASSIFICATION OF REPORT	18. SECURITY CLASSIFICATION OF THIS PAGE	19. SECURITY CLASSIFICATION OF ABSTRACT	20. LIMITATION OF ABSTRACT
Unclassified	Unclassified	Unclassified	UL

NSN 7540-01-280-5500

Standard Form 298 (Rev. 2-89)
Prescribed by ANSI Std. 239-18, 298-102

Approved for public release; distribution is unlimited.

EQUIVALENT IMPEDANCE OF ROUGH SURFACE AT LOW GRAZING ANGLES

Marcelo Jorge de Assis Motta
Lieutenant Commander, Brazilian Navy
B.S.E.E., University of São Paulo, 1990

Submitted in partial fulfillment of the
requirements for the degree of

MASTER OF SCIENCE IN ELECTRICAL ENGINEERING

from the

NAVAL POSTGRADUATE SCHOOL
September 1999

Author: Marcelo Jorge de Assis Motta

Approved by: R. Janaswamy
Ramakrishna Janaswamy, Thesis Advisor

David C. Jenn
David Jenn, Second Reader

Jeffrey B. Knorr, Chairman
Department of Electrical and Computer Engineering

ABSTRACT

Equivalent impedance of a rough surface is determined by solving the problem of radiowave propagation over rough random surface by using the parabolic equation method. We consider horizontal polarization and assume the rough surface, defined by discrete points, to be perfectly conducting. This assumption has minimum effects for frequencies in the VHF band and above. The essential point of this thesis is to solve numerically a Volterra integral equation of the second kind for the surface current. Because the computation becomes very intense for long ranges, we present a multiple sections solution, where the solution procedure is successively repeated for smaller ranges. The numerical results are compared with results available in the literature. Finally, we apply the technique to determine the equivalent impedance of a sinusoidal random rough surface by comparing the resulting normalized field to the field of a 2-ray model over a constant impedance plane.

TABLE OF CONTENTS

ACKNOWLEDGMENT

The author is very grateful to the Brazilian Navy graduation program, which has provided the means for this unique and rewarding educational opportunity. In addition, the author would like to thank the outstanding professors and staff at the Naval Postgraduate School for their tutoring and assistance in his learning endeavors.

A very special thanks is extended to Professor Ramakrishna Janaswamy. His patience, guidance, unique insight and unsurpassed dedication, which he consistently put forward, made possible this work, and many others like it.

I. INTRODUCTION

Low-grazing angle radiowave propagation over random rough surface is an extremely important topic in many areas of interest to the Navy, such as sea-to-sea communications or detection of low-flying targets over the sea surface. Depending on the rough surface characteristics, the direct field and the field reflected and diffracted by the rough surface will interact in different ways, changing the field strength at a certain point of interest. Numerous analytical methods are available for predicting electromagnetic wave propagation over such surfaces, such as physical optics, geometric optics, normal mode analysis and combination of the above. However, a complex surface profile complicates the application of these methods. The Parabolic Equation (PE) method, where a Helmholtz equation is approximated by a parabolic equation, has been extensively used for the determination of forward propagation because of its numerical efficiency. When making this approximation we are assuming that waves travel predominantly in the forward direction and that the back-scattered waves are neglected. This situation is met in many practical propagation problems. Naturally there are situations where it is not possible to apply such an approximation. For example, when there is a large obstacle behind a receiver, the back-scattered field cannot be neglected. The use of the parabolic partial differential equation method allows us to calculate the field at one location in terms of the field at a previous location, utilizing a marching scheme, resulting in a more efficient computational method.

In this thesis we numerically solve a Volterra integral equation of the second kind to predict fields over a rough surface. We consider horizontal polarization and a perfectly conducting rough surface to simplify the formulation. The later assumption will

have minimum effects for frequencies in the VHF band and above. Then we apply the technique developed to determine the equivalent impedance of sinusoidal rough surfaces. This is done by comparing the resulting normalized field to the field of a 2-ray model over a constant impedance plane. A random surface with a fixed spectrum is simulated by translating the sinusoidal surface of given peak-to-peak height and period in a random fashion. This is done by including a phase for the sinusoidal surface and varying it uniformly over $[0,2\pi]$. Finally we show how to generate the rough sea surface according to the *Pierson-Moskowitz spectrum.*

Chapter II describes the theoretical formulation, the numerical solution used to solve the integral equation and the methodology for the equivalent impedance calculation when using parabolic equation. Chapter III presents numerical results, comparing them with practical cases of radiowave propagation over terrain, and calculates the equivalent impedance for a sinusoidal surface. Chapter IV describes how to generate the sea surface according to the *Pierson-Moskowitz spectrum.* Recommendations and conclusions are presented in Chapter V.

II. THEORETICAL FORMULATION

In this chapter we first present a Volterra type integral equation of the second kind for the determination of the surface current on the rough surface based on the parabolic equation approximation. Because a straightforward solution of a Volterra integral equation for long ranges becomes computationally burdensome, we present an alternate technique whereby (i) the range is divided into several sections, (ii) the field is calculated at vertical lines at the junction of two sections, and (iii) the field on a vertical line is used as a source for the determination of current on the next section. The rough surface is defined by discrete points and a linear interpolation between consecutive points is assumed. Figure 1 shows a possible irregular surface. The terrain is assumed to be a perfect electric conductor (conductivity $\rightarrow$ infinite). A 2-dimensional case is considered where the source, geometry and fields are assumed to be invariant in the y direction. Propagation is assumed to take place in the xz plane and is mathematically described by the standard parabolic equation given by

$$\frac{\partial u}{\partial x} = \frac{i}{2k_0}\frac{\partial^2 u}{\partial z^2} \tag{2.1}$$

where 'u' is the reduced field variable and is related to the electrical field 'U' through

$$U(x,z) = e^{ik_0 x}u(x,z),$$

$k_0 = \frac{2\pi}{\lambda}$ is the wave number and λ is the free-space wavelength. An $e^{-i\omega t}$ time dependence is assumed throughout.

The following assumptions are made: (i) the waves are assumed to predominantly travel in the positive x-direction, and (ii) back scattering of waves is ignored. Given a source field, $f(z)$, at $x=0$ one wants to calculate the field at x, where x is the horizontal distance from the source and z is the height with respect to some reference level. An integral representation, similar to Kirchoff's integral form, can be derived based on integrating the parabolic equation in the domain formed by two vertical lines, the rough surface, and an infinite boundary as shown in Figure 1.

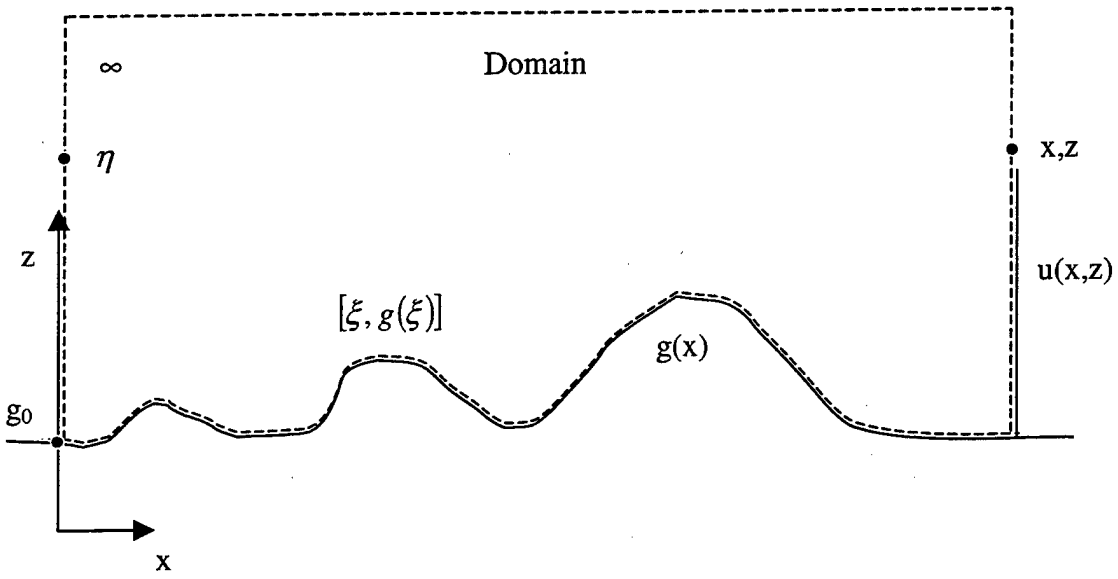

Figure 1: Perfectly Conducting Rough Surface

The field at the point (x,z) is given by [Ref. 1]:

$$u(x,z)=\int_{g_0}^{\infty} f(\eta)G_0[x,z;0,\eta]d\eta-\frac{i}{2k_0}\int_0^x \frac{\partial u_s}{\partial \eta}(\xi)G_0[x,z;\xi,\eta=g(\xi)]d\xi$$

$$\overset{def}{=} u_1(x,z)-u_2(x,z) \qquad (2.2)$$

where $i=\sqrt{-1}$ and $G_0[x,z;\xi,\eta]$ is the Green's function for the basic parabolic equation in free space:

$$G_0[x,z;\xi,\eta]=\sqrt{\frac{k_0}{2\pi(x-\xi)i}}\,e^{\frac{i(z-\eta)^2 k_0}{2(x-\xi)}} \tag{2.3}$$

For later use we will also be interested in the plane-wave spectral representation of the Green's function obtained by decomposing the field in terms of plane waves travelling back and forth along the z-axis:

$$G_0[x,z;\xi,\eta]=\frac{H(x-\xi)}{2\pi}\int_{-\infty}^{\infty} e^{ip(z-\eta)}e^{-i(x-\xi)\frac{p^2}{2k_0}}dp \tag{2.4}$$

where $H(\bullet)$ is the Heaviside step function.

The first integral of Equation 2.2 is performed in the vertical direction using the source field $f(\eta)$. Its lower limit is g_0 and its upper limit is infinite. However, when a numerical computation is required, it will be truncated at some finite height. This integral corresponds to the field produced by the source $f(\eta)$ in free space.

The second integral of Equation 2.2 is performed in the horizontal direction along the rough surface $\eta=g(\xi)$. This integral corresponds to the field reflected and diffracted by the rough surface. The term $\frac{\partial u_s}{\partial \eta}(\xi)$ corresponds to the vertical derivative of the field on the surface and is related to the normal derivative on the rough surface by

$$\frac{\partial u}{\partial z}=\frac{1}{\sqrt{1+[g'(x)]^2}}\frac{\partial u}{\partial n} \tag{2.5}$$

where $g(x)$ is the surface profile, and the prime denotes differentiation with respect to the argument. Whenever we refer to the term *current* we will assume it to mean the

vertical derivative of surface field. An integral equation for $\frac{\partial u_s}{\partial \eta}$ may be formulated by differentiating Equation 2.2 with respect to z and tending z to the surface. Taking the proper limiting values one gets [Ref. 1]:

$$\frac{\partial u_s}{\partial z}(x) = -2 \int_{g_0}^{\infty} f(\eta) \frac{\partial}{\partial \eta} G_0[x, g(x); 0, \eta] d\eta +$$

$$+ \int_0^x \frac{\partial u_s}{\partial \eta}(\xi) \frac{g(x) - g(\xi)}{x - \xi} G_0[x, g(x); \xi, g(\xi)] d\xi \qquad (2.6)$$

where $\int$ denotes a principal value integral.

Equation 2.6 is a Volterra integral equation of the second kind where the current at a given point will depend only on the current at the previous points. Thus we notice the causal property of the Volterra integral equation. In order to solve it we need to use a marching procedure, where we calculate the current at a point based on the current at all other previous points. However, this current calculation becomes computationally very intense for large distances. In order to alleviate this problem, we present the multiple sections solution described on the next section. Once we have the current on the surface, given by Equation 2.6, we can find the field at any point (x, z) using Equation 2.2.

A. MULTIPLE SECTIONS SOLUTION

We can reduce the computation time by dividing the surface into a number of sections and using Equation 2.6 over the sub-intervals. Thus, instead of calculating the current on the entire surface between a transmitter and a location of interest, we can perform current calculations successively on shorter sections by making use of field data available on vertical lines.

Given the field on a vertical line, the following procedure is performed in order to calculate the field on the next vertical line:

Step 1: Calculate the *incident current* induced on the rough surface by the initial field. The incident current on the surface is given by the first term on the right hand side in Equation 2.6.

Step 2: Calculate the *total current* on the rough surface. The total current on the surface is given by both terms on the right hand side of Equation 2.6.

Step 3: Calculate the *field* at the next vertical line, utilizing Equation 2.2.

We notice a trade off when applying this split-section method, illustrated on Figure 2. On one hand we reduce the calculation time needed to solve the Volterra integral equation since we are dealing with smaller distances in each individual section. On the other hand, it will be necessary to calculate the field on vertical lines at intermediate sections. There will be an optimum number of sections, where the total computation time will be minimized.

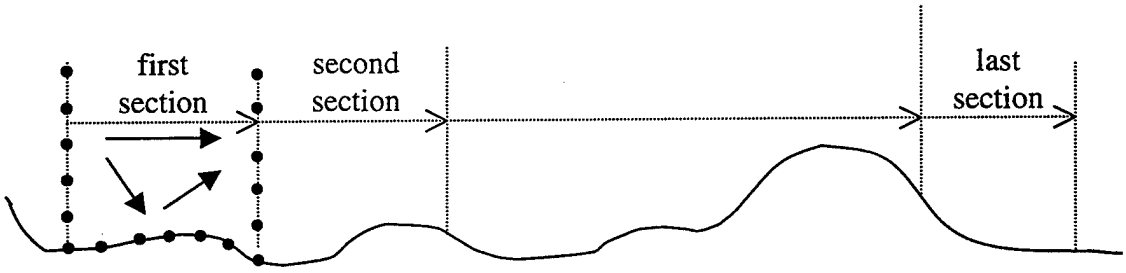

Figure 2: Representation of the Multiple Sections Solution

B. INITIAL FIELD SPECIFICATION

In order to be able to band limit the initial data as well as to account for finite antenna beamwidths we use a Gaussian spatial distribution given by:

$$u(0,z) = Ae^{-\frac{(z-z_t)^2}{2\sigma_z^2}} \tag{2.7}$$

where z_t is the transmitting antenna height, σ_z is it standard deviation for the Gaussian distribution and is related to the antenna beamwidth in the vertical plane through

$$BW_{3dB} = 2\tan^{-1}\left(\frac{0.833}{k_0\sigma_z}\right)$$

and A is the amplitude. Obviously, choosing a small σ_z (for example $\lambda/2$) makes the source field very concentrated around z_t. Notice Figure 37 (upper figure) where we have the source field as a function of σ_z.

Using this source field as $f(\eta)$ in the first integral in Equation 2.2 we find that the free space field, which corresponds to the first integral of Equation 2.2, is given by:

$$u_{free-space}(x,z) = \frac{A\sigma_z}{\sqrt{\sigma_z^2 + \frac{ix}{k_0}}} e^{-\frac{(z-z_t)^2}{2\left(\sigma_z^2+\frac{ix}{k_0}\right)}} \tag{2.8}$$

Given the source field described by Equation 2.8 we can also calculate its derivative at (x,z) with respect to z:

$$\frac{\partial u}{\partial z}(x,z) = \frac{-A\sigma_z(z-z_t)}{\left[\sigma_z^2 + \frac{ix}{k_0}\right]^{3/2}} e^{-\frac{(z-z_t)^2}{\left[2\left(\sigma_z^2+\frac{ix}{k_0}\right)\right]}} \tag{2.9}$$

C. NUMERICAL SOLUTION PROCEDURE

1. Calculation of the Incident Current on the Rough Surface

a. Calculation for the First Section

The incident current on the surface is given by the first term on the right hand side in Equation 2.6.

$$J_{inc}(x) = -2\int_{g_0}^{\infty} f(\eta)\frac{\partial}{\partial \eta} G_0[x, g(x); 0, \eta]d\eta \tag{2.10}$$

For the first section we have an analytical expression for $f(\eta)$, given by Equation 2.7. Substituting $z = g(x)$, taking the derivative with respect to η in Equation 2.3, and using this result and Equation 2.7 into the right hand side of Equation 2.10, we find the expression for the incident current on the rough surface. This expression is valid only for the first section where an analytical expression for the initial field is available:

$$J_{inc}(x) = \frac{-2A\sigma_z[g(x) - z_t]}{\left[\sigma_z^2 + \frac{ix}{k_0}\right]^{3/2}} e^{\frac{[g(x)-z_t]^2}{\left[2\left(\sigma_z^2 + \frac{ix}{k_0}\right)\right]}} \tag{2.11}$$

b. Calculation for the Remainder Sections

For the remainder steps we need to perform a numerical evaluation of the incident current, given by Equation 2.10. The use of trapezoidal rule is not suitable because the Green's function term inside the integral in Equation 2.10 has a phase term of the type $\frac{1}{x}$, and for small distances x it introduces numerical errors. As a result, a more sophisticated integration technique is required.

Making use of the spectral representation in Equation 2.4 we rewrite the expression for $J_{inc}(x)$ as:

$$J_{inc}(x)=\frac{iH(x)}{\pi}\int_{g_0}^{\infty} f(\eta)\int_{-\infty}^{\infty} p e^{ip[g(x)-\eta]} e^{-\frac{ip^2 x}{2k_0}} dp \tag{2.12}$$

Interchanging the orders of integration and substituting $\eta = g_0 + \xi$ we get:

$$J_{inc}(x)=\frac{i}{\pi}H(x)\int_{-\infty}^{\infty} p e^{ip[g(x)-g_0]} e^{-\frac{ip^2 x}{2k_0}} dp \int_{0}^{\infty} f(g_0+\xi) e^{-ip\xi} d\xi$$

$$\stackrel{def}{=}\frac{i}{\pi}H(x)\int_{-\infty}^{\infty} p e^{ip[g(x)-g_0]} e^{-\frac{ip^2 x}{2k_0}} \Im(p) dp \tag{2.13}$$

where $\Im(p)=\int_{0}^{\infty} f(g_0+\xi) e^{-ip\xi} d\xi$ is the Fourier transform of the initial field.

Since the parabolic equation has a limited angular response [Ref. 2], we need to truncate the integration limits in Equation 2.13 at $\pm p_{\max}$, where $p_{\max}$ is of the order of $k_0 sin(\theta_{\max})$ where $\theta_{\max} \approx 15^{\circ}$. Because we are truncating the integral in Equation 2.13, we need to introduce a filter, such as a Hanning filter, in order to smoothly roll-off the function. The expression for J_{inc} then becomes:

$$J_{inc}(x)\approx\frac{i}{\pi}\int_{-p_{\max}}^{p_{\max}} W(p) p \Im(p) e^{-\frac{ip^2 x}{2k_0}} e^{ip[g(x)-g_0]} dp \tag{2.14}$$

where $W(p)$ is the Hanning filter. The above integral will be evaluated numerically by the trapezoidal rule. The Hanning filter is an even function and its discrete form is given by:

$$W(p=m\Delta p)=\begin{cases}1, 0\le m\le \frac{3}{8}M \\ sin^2\left(\frac{4\pi m}{N}\right), \frac{3}{8}m\le p\le M\end{cases}$$

where M is the number of points used in the discrete Fourier transform. The final numerical expression for J_{inc} is:

$$J_{inc}(x)=\frac{i\Delta p}{\pi}\sum_{m=1}^{M}W(p_m)p_m\Im(p_m)e^{-\frac{ip_m^2x}{2k_0}}e^{ip_m[g(x)-g_0]} \tag{2.15}$$

where $p_m=m\Delta p$.

2. Calculation of the Total Current on the Rough Surface

Once we calculate the incident current on the rough surface, the next step is to calculate the total current on the surface. The total current on the surface is represented by Equation 2.6. We can say for the clarity of explanation that $J(x)=\frac{\partial u_s}{\partial z}(x)$ and $J(\xi)=\frac{\partial u_s}{\partial \eta}(\xi)$. Defining $g_d(x;\xi)=\frac{g(x)-g(\xi)}{x-\xi}$ we can rewrite Equation 2.6 as:

$$J(x)=J_{inc}(x)+\sqrt{\frac{k_0}{2\pi i}}\int_0^x J(\xi)\frac{g_d(x;\xi)}{\sqrt{x-\xi}}e^{ik_0\frac{x-\xi}{2}g_d^2(x;\xi)}d\xi \tag{2.16}$$

where $J_{inc}(x)$ is given by Equation 2.10.

The second term on the right-hand side in Equation 2.16 can be broken in N sub-integrals:

$$J(x) = J_{inc}(x) + \sum_{n=1}^{N} \sqrt{\frac{k_0}{2\pi i}} \int_{(n-1)\delta}^{n\delta} J(\xi) \frac{g_d(x;\xi)}{\sqrt{x-\xi}} e^{i\frac{k_0}{2}(x-\xi)g_d^2(x;\xi)} d\xi$$

$$\stackrel{def}{=} J_{inc}(x) + \sum_{n=1}^{N} \sqrt{\frac{k_0}{2\pi i}} I_n \qquad (2.17)$$

where $I_n = \int_{(n-1)\delta}^{n\delta} J(\xi) \frac{g_d(x;\xi)}{\sqrt{x-\xi}} e^{i\frac{k_0}{2}(x-\xi)g_d^2(x;\xi)} d\xi$.

Notice from Figure 3 below that the following notation has been adopted:

$$n = 1,2,3,..., N+1$$

$$x_n = (n-1)\delta$$

$$x_{N+1} = N\delta = x$$

$$x - \delta = x_N = (N-1)\delta$$

$$g_n = g(x_n)$$

$$J_n = J(x_n)$$

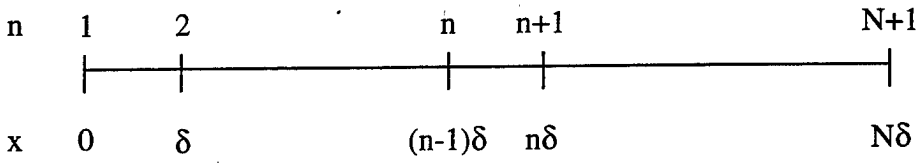

Figure 3: Nomenclature for the discretization process

With reference to the Figure 4, we can approximate $g_d(x;\xi) = \frac{g(x)-g(\xi)}{x-\xi}$ as

$g_{dn} = \frac{g(x) - g(x_{n+1/2})}{x - x_{n+1/2}}$, where $x_{n+1/2} = (n - \frac{1}{2})\delta$ and $g(x_{n+1/2}) \approx \frac{g_n + g_{n+1}}{2}$. Also we can

approximate the variable ξ in $g_d(x;\xi)$, located between $x_n=(n-1)\delta$ and $x_{n+1}=n\delta$ by $x_{n+1/2}=(n-\frac{1}{2})\delta$, and the function value $g(\xi)$, located between g_n and g_{n+1} by $g(x_{n+1/2})$.

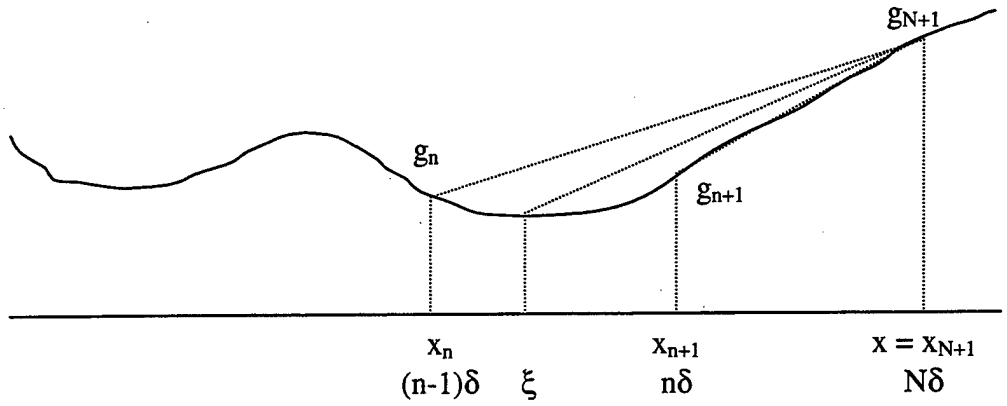

Figure 4: Approximation for $g_d(x;\xi)$

Letting $\xi=\tau\delta+(n-1)\delta$, in Equation 2.17, where $0<\tau<1$ in the nth segment, and approximating $J(\xi)$ linearly between J_n and J_{n+1} as $J(\xi)=(J_{n+1}-J_n)\tau+J_n$, we simplify the expression for I_n as:

$$I_n = g_{dn}\sqrt{\delta}\,e^{i\frac{k_0}{2}\delta g_{dn}^2(N+1-n)}\int_0^1[(J_{n+1}-J_n)\tau+J_n]\frac{e^{-i\frac{k_0\delta}{2}g_{dn}^2\tau}}{\sqrt{(N+1-n)-\tau}}d\tau \qquad (2.18)$$

The result may be expressed in terms of the Fresnel integral as [Ref. 1]:

$$I_n = 2\sqrt{\frac{\pi}{k_0}}\,\mathrm{sgn}(g_{dn})\{\left\{\left((J_{n+1}-J_n)(N+1-n)+J_n+\frac{\pi(J_{n+1}-J_n)}{ik_0\delta g_{dn}^2}\right)[F(t_2)-F(t_1)]\right\}-$$

$$-\frac{(J_{n+1}-J_n)}{ik_0\delta g_{dn}^2}e^{i\frac{\pi}{2}t_1^2}\left[t_2e^{i\frac{k_0}{2}\delta g_{dn}^2}-t_1\right]\Bigg\}\ \text{for } g_{dn\neq 0}, \text{ and } I_n=0 \text{ for } g_{dn}=0 \qquad (2.19)$$

where

$$\operatorname{sgn}(x)=\begin{cases}+1, x>0\\ 0, x=0\\ -1, x<0\end{cases}$$

$$t_1=\sqrt{\frac{k_0\delta(N-n)}{\pi}}\,|g_{dn}|$$

$$t_2=\sqrt{\frac{k_0\delta(N+1-n)}{\pi}}\,|g_{dn}|$$

and

$$F(t)=\int_0^t e^{i\frac{\pi}{2}x^2}\,dx \text{ is the complex Fresnel integral.} \tag{2.20}$$

Once we have the expression for I_n we can calculate the total current on the surface using Equation 2.17:

$$J_{N+1}=J_{inc(N+1)}+\sqrt{\frac{2}{i}}\operatorname{sgn}(g_{dn})\sum_{n=1}^{N-1}\left\{\left[(J_{n+1}-J_n)(N+1-n)+J_n-\frac{i(J_{n+1}-J_n)}{k_0\delta g_{dn}^2}\right][F(t_2)-F(t_1)]+\right.$$
$$\left.+\frac{i(J_{n+1}-J_n)}{k_0\delta g_{dn}^2}e^{i\frac{\pi}{2}t_1^2}\left(t_2e^{i\frac{k_0}{2}\delta g_{dn}^2}-t_1\right)\right\}+I_N \tag{2.21}$$

where

$$I_N=2\operatorname{sgn}(g_{N+1}-g_N)\sqrt{\frac{\pi}{k_0}}\times$$

$$\times\left\{\left[F(t_2)\left(1+\frac{1}{i\pi t_2^2}\right)-e^{i\frac{\pi}{2}t_2^2}\right]J_{N+1}+\frac{J_N}{i\pi t_2}\left(e^{i\frac{\pi}{2}t_2^2}-\frac{F(t_2)}{t_2}\right)\right\}. \tag{2.22}$$

In Equation 2.22 we notice that $I_N=0$ whenever $g_N=g_{N+1}$.

Combining Equations 2.21 and 2.22 we have the final expression for the current on the surface:

$$J_{N+1}=\frac{J_{inc(N+1)}}{1-\sqrt{\frac{k_0}{2\pi i}}a_1}+\frac{\sqrt{\frac{k_0}{2\pi i}}b_1}{1-\sqrt{\frac{k_0}{2\pi i}}a_1}J_N+\sqrt{\frac{2}{i}}\frac{1}{1-\sqrt{\frac{k_0}{2\pi i}}a_1}$$

$$\sum_{n=1}^{N-1}\left\{\left[(J_{n+1}-J_n)(N+1-n)+J_n-\frac{i(J_{n+1}-J_n)}{k_0\delta g_{dn}^2}\right][F(t_2)-F(t_1)]+\right.$$

$$\left.\frac{i(J_{n+1}-J_n)}{k_0\delta g_{dn}^2}e^{i\frac{\pi}{2}t_1^2}\left(t_2e^{i\frac{k_0}{2}\delta g_{dn}^2}-t_1\right)\right\} \qquad (2.23)$$

where the coefficients a_1 and b_1 are given by:

$$a_1=2\,\mathrm{sgn}(g_{N+1}-g_N)\sqrt{\frac{\pi}{k_0}}\left\{F(t_2)\left(1+\frac{1}{i\pi t_2^2}\right)-\frac{e^{i\frac{\pi}{2}t_2^2}}{i\pi t_2}\right\}$$

$$b_1=2\,\mathrm{sgn}(g_{N+1}-g_N)\sqrt{\frac{\pi}{k_0}}\frac{1}{i\pi t_2}\left\{e^{i\frac{\pi}{2}t_2^2}-\frac{F(t_2)}{t_2}\right\}$$

3. Calculation of the Field

Once we have the total current on the rough surface we can calculate the field at any x. In Equation 2.2 we notice that $u_1(x,z)$ corresponds to the incident field and $u_2(x,z)$ corresponds to the field reflected and diffracted by the rough surface.

a. Calculation of the Incident Field

The incident field, corresponding to the first integral on the right hand side of Equation 2.2 and given by $u_1(x,z)=\int_{go}^{\infty}f(\eta)G_0[x,z;0,\eta]d\eta$ will be calculated using the same technique as used for the calculation of $J_{inc}(x)$. It is given by:

$$u_1(x,z)=\frac{1}{2\pi}\int_{-\infty}^{\infty}\Im(p)e^{-\frac{ip^2x}{2k_0}}e^{ip(z-g_0)}dp \qquad (2.24)$$

As before, a Hanning filter is introduced into the expression when the limits of the integral are truncated. The expression for $u_1(x,z)$ then becomes:

$$u_1(x,z) \approx \frac{1}{2\pi} \int_{-p_{\max}}^{p_{\max}} W(p)\Im(p) e^{-\frac{ip^2 x}{2k_0}} e^{ip(z-g_0)} dp \tag{2.25}$$

Finally we can apply the trapezoidal rule to Equation 2.25, obtaining the final numerical expression for $u_1(x,z)$:

$$u_1(x,z) = \frac{\Delta p}{2\pi} \sum_{n=1}^{N} W(p_n)\Im(p_n) e^{-\frac{ip_n^2 x}{2k_0}} e^{ip_n(z-g_0)} \tag{2.26}$$

b. Calculation of the Field Reflected and Diffracted by the Rough Surface

The field reflected and diffracted by the rough surface, corresponding to the second integral on the right hand side of Equation 2.2 and given by

$$u_2(x,z) = \frac{i}{2k_0} \int_0^x \frac{\partial u_s}{\partial \eta}(\xi) G_0[x,z;\xi,\eta = g(\xi)] d\xi \tag{2.27}$$

cannot be calculated by applying the trapezoidal rule directly because the Green's function has a singularity at $x = \xi$. This singularity must be extracted apriori before performing the integration. We can rewrite the above expression for $u_2(x,z)$ as:

$$u_2(x,z) = \sqrt{\frac{i}{8\pi k_0}} \int_0^x \frac{J(\xi)}{\sqrt{x-\xi}} e^{i\frac{[z-g(\xi)]^2 k_0}{2(x-\xi)}} d\xi \tag{2.28}$$

We replace $[z-g(\xi)]$ by $[z-g(x)+g(x)-g(\xi)]$ in Equation 2.28 and define:

$$K(x;\xi) = J(\xi) e^{ik_0[z-g(x)]\frac{g(x)-g(\xi)}{(x-\xi)}} e^{i\frac{k_0[g(x)-g(\xi)]^2}{2(x-\xi)}} \tag{2.29}$$

so that

$$K(x;x)=J(x)e^{ik_0 g'(x)(z-g(x))} \tag{2.30}$$

If $g(x)$ is continuous $K(x;\xi)$ is well behaved as $x\to\xi$. We can rewrite Equation 2.28 as:

$$u_2(x,z)=\sqrt{\frac{i}{8\pi k_0}}\times$$

$$\times\left[K(x;x)\int_0^x \frac{e^{ik_0\frac{[z-g(x)]^2}{2(x-\xi)}}}{\sqrt{x-\xi}}d\xi+\int_0^x \frac{K(x;\xi)-K(x;x)}{\sqrt{x-\xi}}e^{ik_0\frac{[z-g(x)]^2}{2(x-\xi)}}d\xi\right] \tag{2.31}$$

By a change of variables, the first term within square brackets of Equation 2.31 can be solved in terms of the Fresnel integral resulting in [Ref. 1]:

$$u_2(x,z)=\sqrt{\frac{i}{8\pi k_0}}\left\{K(x;x)I_1(x,z)+\int_0^x \frac{K(x;\xi)-K(x;x)}{\sqrt{x-\xi}}e^{i\frac{k_0}{2}\frac{[z-g(x)]^2}{(x-\xi)}}d\xi\right\} \tag{2.32}$$

where:

$$I_1(x,z)=2\sqrt{x}e^{i\frac{k_0}{2}\frac{[z-g(x)]^2}{x}}-$$

$$-(1-i)\sqrt{\pi k_0}[z-g(x)]\left\{1-(1-i)F\left(\sqrt{\frac{k_0}{\pi x}}[z-g(x)]\right)\right\} \tag{2.33}$$

The integral in Equation 2.32 can now be evaluated by applying the trapezoidal rule to the second term on the right hand side, since the singularity at $x=\xi$ has been extracted.

4. Fresnel Integral Calculation

For small arguments (smaller than or equal than 0.1) the Fresnel integral can be approximated by

$$F(x)=x+\frac{i\pi}{6}x^3 \tag{2.34}$$

This expression is obtained by taking the limit when $t\to 0$ in Equation 2.20. Using this approximation will reduce CPU time somewhat. For arguments greater than 0.1, the Fresnel integral will be calculated by a rational approximation given in [Ref. 3]:

$$F(x)=C(x)+iS(x)\approx\frac{1}{2}(1+i)-[ir(x)+s(x)]e^{i\frac{\pi}{2}x^2} \tag{2.35}$$

where

$$r(x)=\frac{1+0.926x}{2+1.792x+3.104x^2}+\varepsilon(x)$$

$$s(x)=\frac{1}{2+4.142x+3.492x^2+6.670x^3}+\varepsilon(x)$$

where $$|\varepsilon(x)|\le 2\times 10^{-3}$$

D. DETERMINATION OF THE EQUIVALENT IMPEDANCE

Once we have determined the field on a vertical line distant x from the source, we can find the equivalent ground impedance that would produce the same field when solving the propagation problem using a two-ray model.

For horizontal polarization, the reflection coefficient for plane waves incident from air on to a non-magnetic lossy, planar interface having an impedance $\eta=\frac{\eta_0}{\sqrt{\epsilon_{rc}}}$ is:

$$\Gamma=\frac{\sin\psi-\sqrt{\epsilon_{rc}}}{\sin\psi+\sqrt{\epsilon_{rc}}}. \tag{2.36}$$

where ψ is the grazing angle such that

$$\tan\psi=\frac{H_t+H_r}{d}$$

$$\approx \sin\psi \text{ for } H_t + H_r \leq \frac{d}{2}$$

and η_0 is the intrinsic impedance of the free-space.

When considering the two-ray model the resultant field will be given by:

$$u = \frac{e^{ik_0 r_1}}{r_1} + \Gamma \frac{e^{ik_0 r_2}}{r_2} \approx u_0 \left\{ 1 + \frac{r_1}{r_2} \Gamma e^{ik_0 (r_2 - r_1)} \right\} \tag{2.37}$$

where r_1 is the line-of-sight path, r_2 is the reflected path and u_0 is the free-space field.

For large distances ($d >> H_t + H_r$) we can approximate $r_2 \approx r_1$ for the amplitude term, and use $r_2 - r_1 \approx \frac{2H_t H_r}{d}$ for the phase term. We can rewrite Equation 2.37 as

$$\frac{u}{u_0} = 1 + \Gamma e^{ik_0 (r_2 - r_1)} \tag{2.38}$$

and express the reflection coefficient as:

$$\Gamma = \left(\frac{u}{u_0} - 1 \right) e^{\frac{i2k_0 H_t H_r}{d}} \tag{2.39}$$

If we now combine Equations 2.36 and 2.39 we have the final expression for $\sqrt{\epsilon_{rc}}$ as a function of the geometry and the normalized field:

$$\sqrt{\epsilon_{rc}} = \sin\psi \left(\frac{e^{\frac{i2k_0 H_t H_r}{d}} + 1 - \frac{u}{u_0}}{e^{\frac{i2k_0 H_t H_r}{d}} - 1 + \frac{u}{u_0}} \right) \tag{2.40}$$

Figure 5 below illustrates the geometry mentioned above.

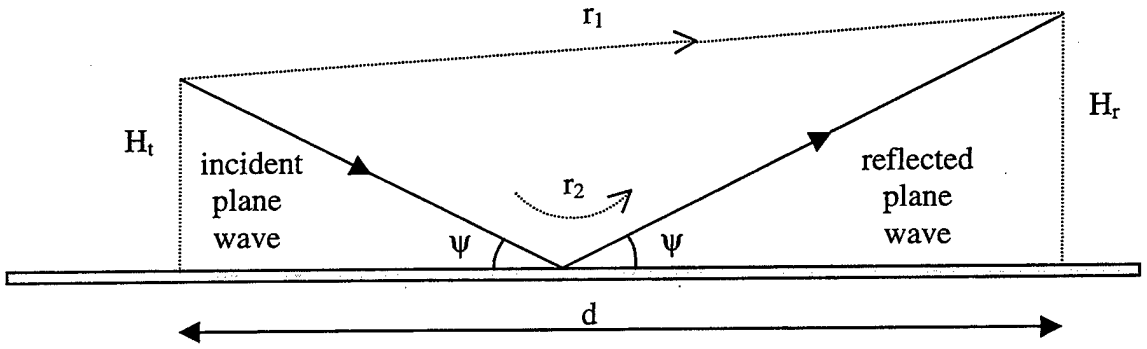

Figure 5: Reflection of Plane wave over Flat Surface

Note that the heights H_t and H_r are relative to the equivalent flat plane, which is normally taken to coincide with the mean of the rough surface. If only one section is used in the PE modeling we can take advantage of the Gaussian representation of the initial field. A somewhat better approximation to Equation 2.37 will then be:

$$\sqrt{\epsilon_{rc}} = \sin\psi \frac{e^{i\frac{2k_0 H_t H_r}{x}\left(1+i\frac{k_0\sigma_z^2}{x}\right)} - \left(\frac{u(x,H_r)}{u_0(x,H_r)} - 1\right)}{e^{i\frac{2k_0 H_t H_r}{x}\left(1+i\frac{k_0\sigma_z^2}{x}\right)} + \left(\frac{u(x,H_r)}{u_0(x,H_r)} - 1\right)} \tag{2.41}$$

III. RESULTS

Having introduced the theoretical formulation in Chapter II, we will present here numerical results obtained with the algorithm developed and compare those with other techniques for some practical cases of radiowave propagation over terrain. We will be comparing the propagation factor (PF) (excess loss over the free space case) obtained with our approach versus the propagation factor obtained from results available in the literature. A positive (negative) value of propagation factor implies gain (loss) with respect to propagation in free space.

A. PROPAGATION OVER A PERFECT ELECTRIC CONDUCTOR PLANE

Consider a transmitter 5 m above flat perfect electric conductor (PEC) ground ($z_t = 5$). One wants to calculate the PF on a vertical line distant 400 m from the transmitter, as shown in Figure 6. The maximum receiver height to be evaluated is 100 m.

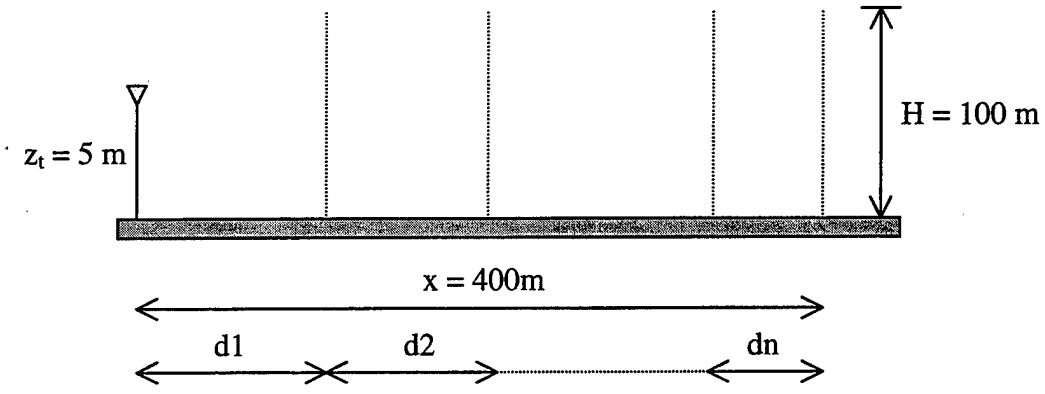

Figure 6: Propagation over a Flat PEC Surface

The PF is defined as:

$$PF\ [dB] = 10\log_{10}\left(\frac{u(x,z)}{u_0(x,z)}\right) \tag{3.1}$$

where $u(x,z)$ and $u_0(x,z)$ are defined in Equations 2.2 and 2.8 respectively.

For a point source above a PEC plane an analytical solution can be obtained by image theory. Using the expression valid in the far field for $x >> z_t, z$, we get

$$PF = \left|\frac{u}{u_0}\right| = 2\left|\sin\left(\frac{k_0 z z_t}{x}\right)\right|.$$

Figure 7 shows a comparison between the two methods for a frequency of operation of 1 GHz and performing the computation using one section. For this range of 400 m good agreement is seen for heights up to 60 m. This result is expected, since the 2-ray model and the PE model use approximations that are valid for horizontal distance large compared to antenna heights. If we move the receiver vertical line further to the right on Figure 6, thereby, increasing the distance from the source, we will have better agreement at higher heights.

On Table 3.1 we have the relationship between the CPU time (Pentium MMX 200 MHz) and the number of sections used in the calculation of the field over a total distance of 400 m. The code was implemented in *MATLAB*. The column *% time* refers to a relative measure to the maximum measured time. We notice that as we change the number of sections from one to two and from two to three the CPU time decreases. However, as we move from three to four sections the CPU time increases. Of course changing the section length will make the CPU time change too. Compare in Table 3.1 cases two and three, both using 2 sections; cases four and five, both using 3 sections and cases six and seven, both using 4 sections. Figure 8 illustrates this dependence. These numbers are influenced by many factors, some dependent on the set-up of the problem

(number of points on the vertical direction, for example) and some dependent on the computer configuration (available memory, for example).

We also notice that it is not possible to choose the sections too small, since it would mean that waves would have to travel at large angles to reach large vertical heights and the parabolic equation has an angular limitation around 15°. Referring to Figure 9 we notice that the results for the cases 3, 5 and 7 are smoother than 2, 4 and 6 respectively. This is because the fields on a vertical line get more accurate as the horizontal distance from the source increases.

We can make a better check to our numerical solution by comparing it with the solution for Gaussian sources instead of the point sources used above. For a Gaussian source, described by Equation 2.7, an analytical expression for the total field over a ground plane is:

$$u(x,z)=\frac{A\sigma_z}{\sqrt{\sigma_z^2+\frac{ix}{k_0}}}\left[e^{-\frac{(z-z_t)^2}{2\left(\sigma_z^2+\frac{ix}{k_0}\right)}}-e^{-\frac{(z+z_t)^2}{2\left(\sigma_z^2+\frac{ix}{k_0}\right)}}\right]$$

where the first term on the right hand side corresponds to the free-space field and the second term corresponds to the field generated by the image source. The PF will be given by

$$PF=\left|1-e^{-\frac{2zz_t}{\left(\sigma_z^2+\frac{ix}{k_0}\right)}}\right| \qquad (3.2)$$

Figure 10 shows current and the propagation factor for Case 2 (d1 = d2 = 200 m). There we notice a small oscillatory behavior for the current. Compare this figure with

Figure 7, where the calculations were performed in one single section. It is seen that the results are smoother. Below we offer an analysis of this behavior.

Figure 11 compares the propagation factor at the end of the first section in Case 2 (d1 = d2 = 200 m), when using our numerical solution and using the image theory with Gaussian source as described by Equation 3.2. We notice such a good agreement, even for large heights, that it is hard to distinguish the two curves. Figure 12 compares the magnitude and the phase of the field at the end of the first section. For the sake of clarity we present Figure 13 that contains basically the same information as Figure 12 but over a smaller vertical scale. There we compare our numerical solution with the solution obtained using the image theory described above. We notice a very good agreement, which indicates that the field at the end of the first section is being calculated correctly. As a result, we conclude that although the multiple section solution improves the speed of the calculation, it introduces some numerical errors, since the PF for Case 1 and Case 2 are not the same, and the only difference between the two cases is that in Case 2 we performed the computation in two sections. In Section 3.C we will see that as we decrease the length of the first section the results become worse.

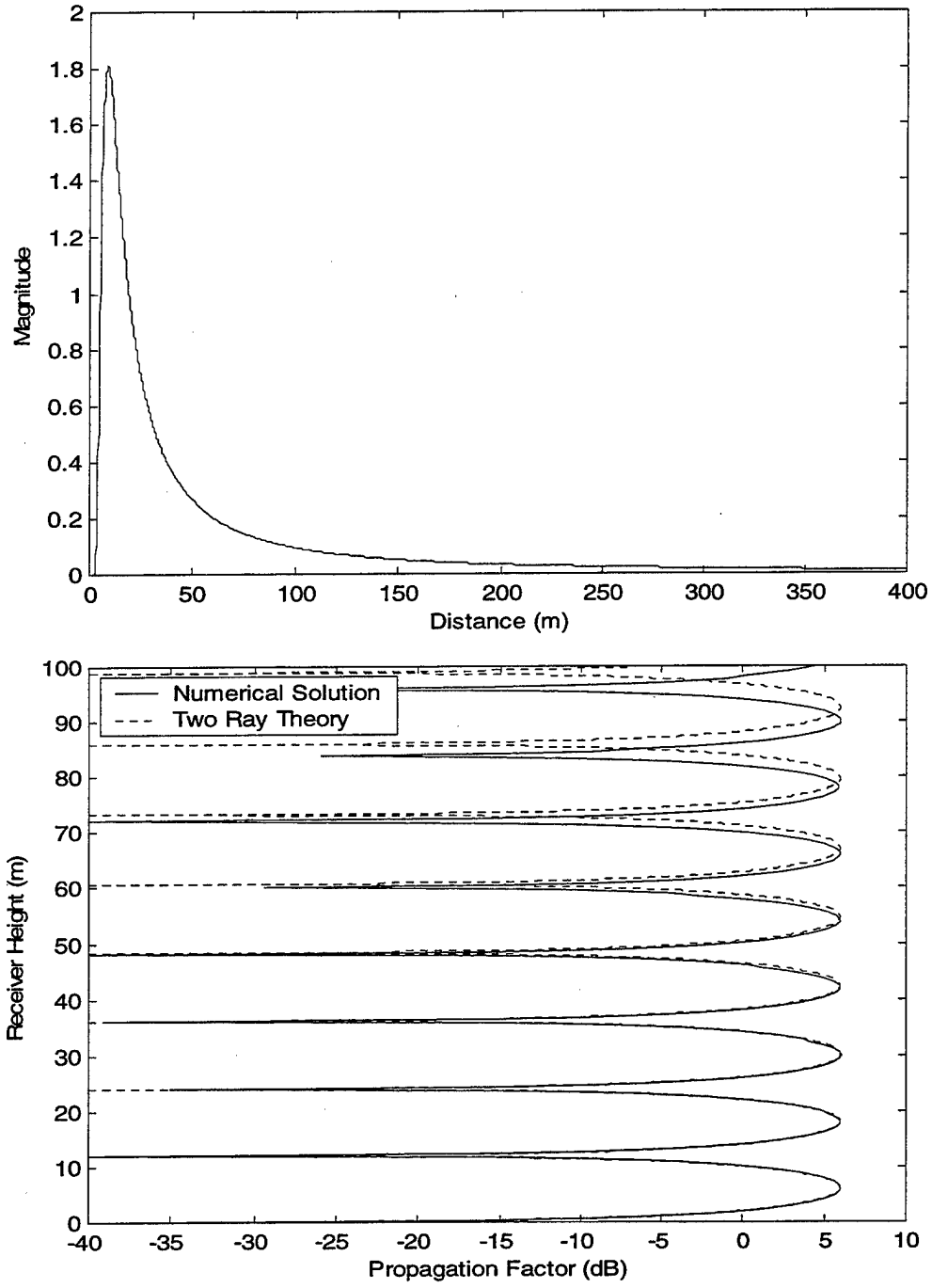

Figure 7: Current (Upper Figure) and Propagation Factor (Lower Figure). Transmitter antenna height is 5 m. Flat earth, frequency = 1 GHz, $\Delta_x = \frac{\lambda}{2}$.

Case	N. of sections	CPU time (sec)	% time	Section Size (m)			
				d1	d2	d3	d4
1	1	1.0177×10^3	100	400	-----	-----	-----
2	2	743.5800	73	200	200	-----	-----
3	2	833.7700	82	300	100	-----	-----
4	3	638.2300	63	200	100	100	-----
5	3	544.2000	53	240	80	80	-----
6	4	646.9100	64	200	100	50	50
7	4	651.4100	64	240	60	50	50

Table 3.1: CPU time for Propagation over PEC Flat Surface

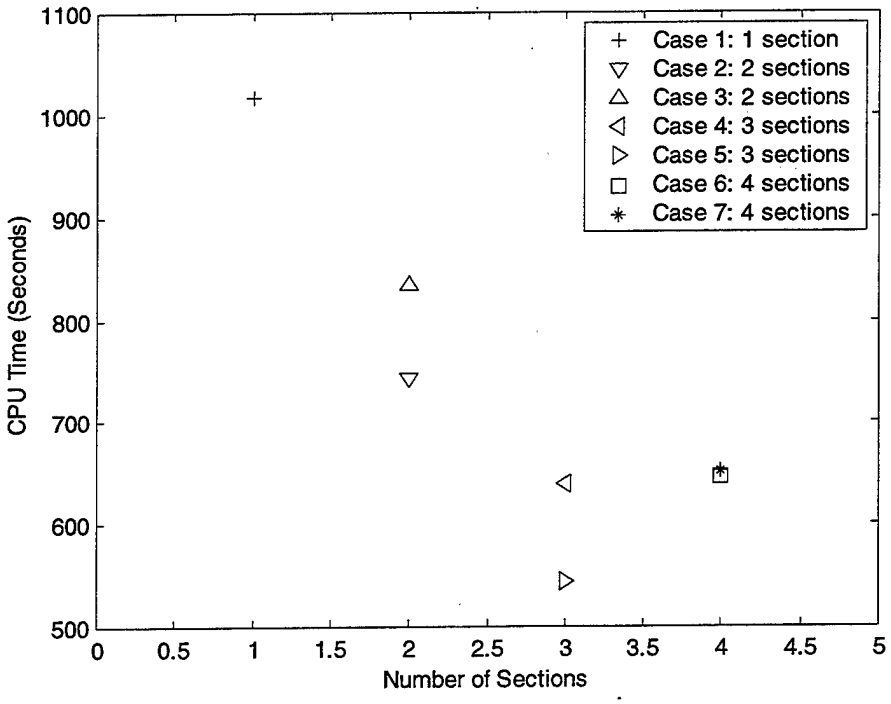

Figure 8: CPU Time as a Function of Number of Sections for the PEC Flat Surface Case

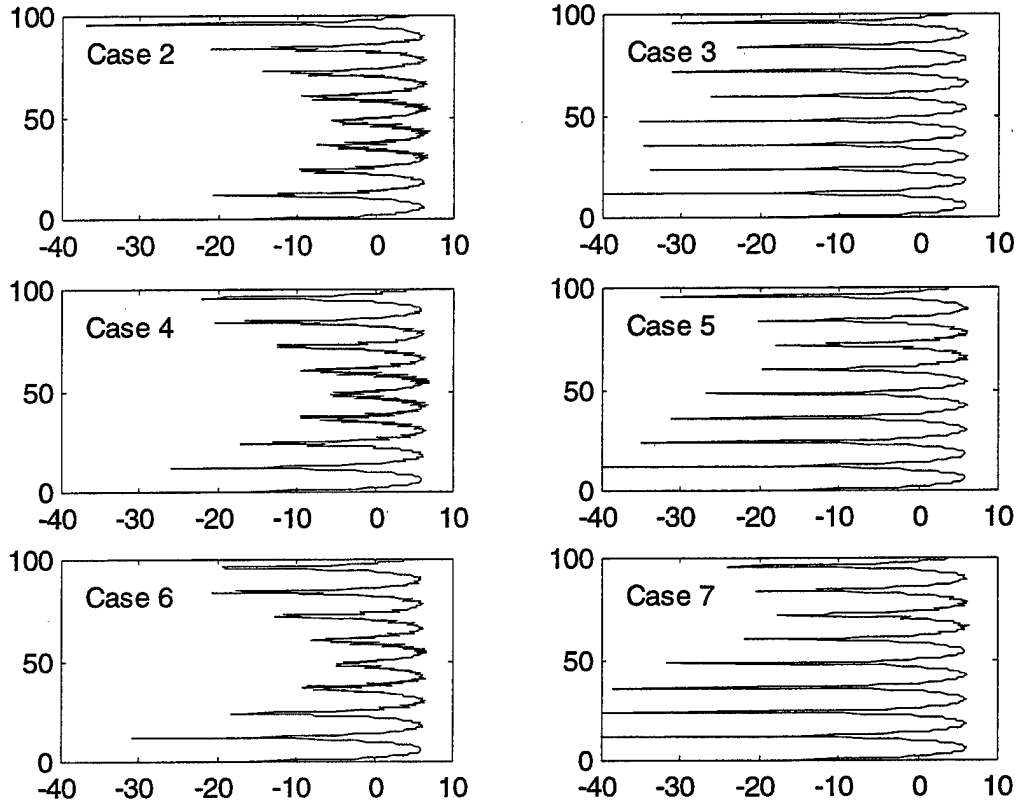

Figure 9: Propagation Factor as a Function of the Number of Sections (x-axis: PF in dB, y-axis: Receiver Height in meters).

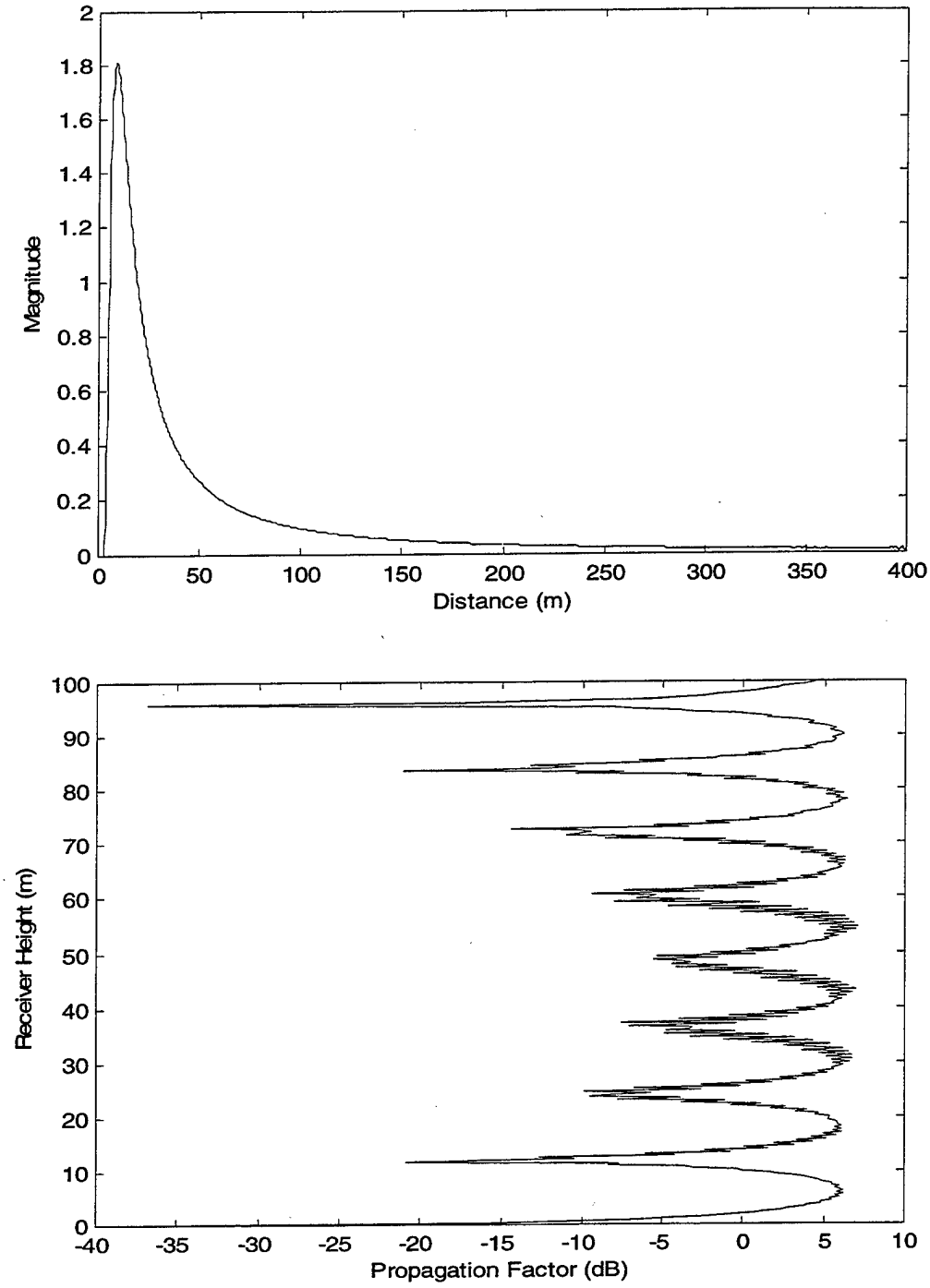

Figure 10: Current (Upper Figure) and Propagation Factor (Lower Figure) for the Case 2 of Flat Surface. Transmitter antenna height is 5 m. Frequency = 1 GHz, $\Delta_x = \frac{\lambda}{2}$.

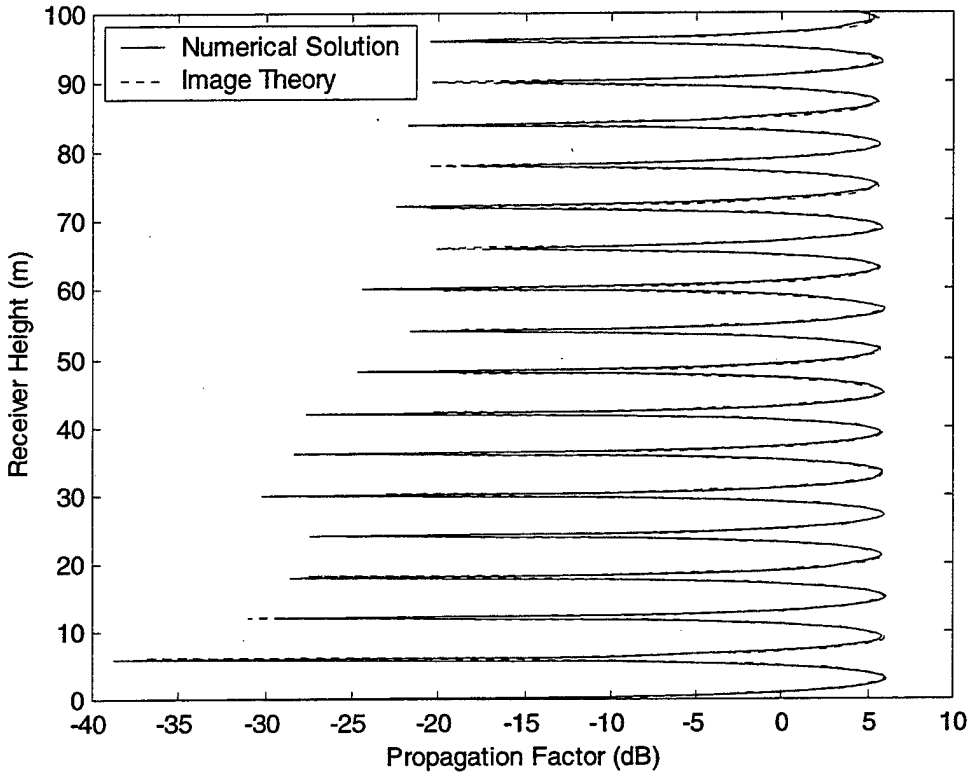

Figure 11: Propagation Factor, Calculated at the End of the First Section of Case 2 of Flat Surface.

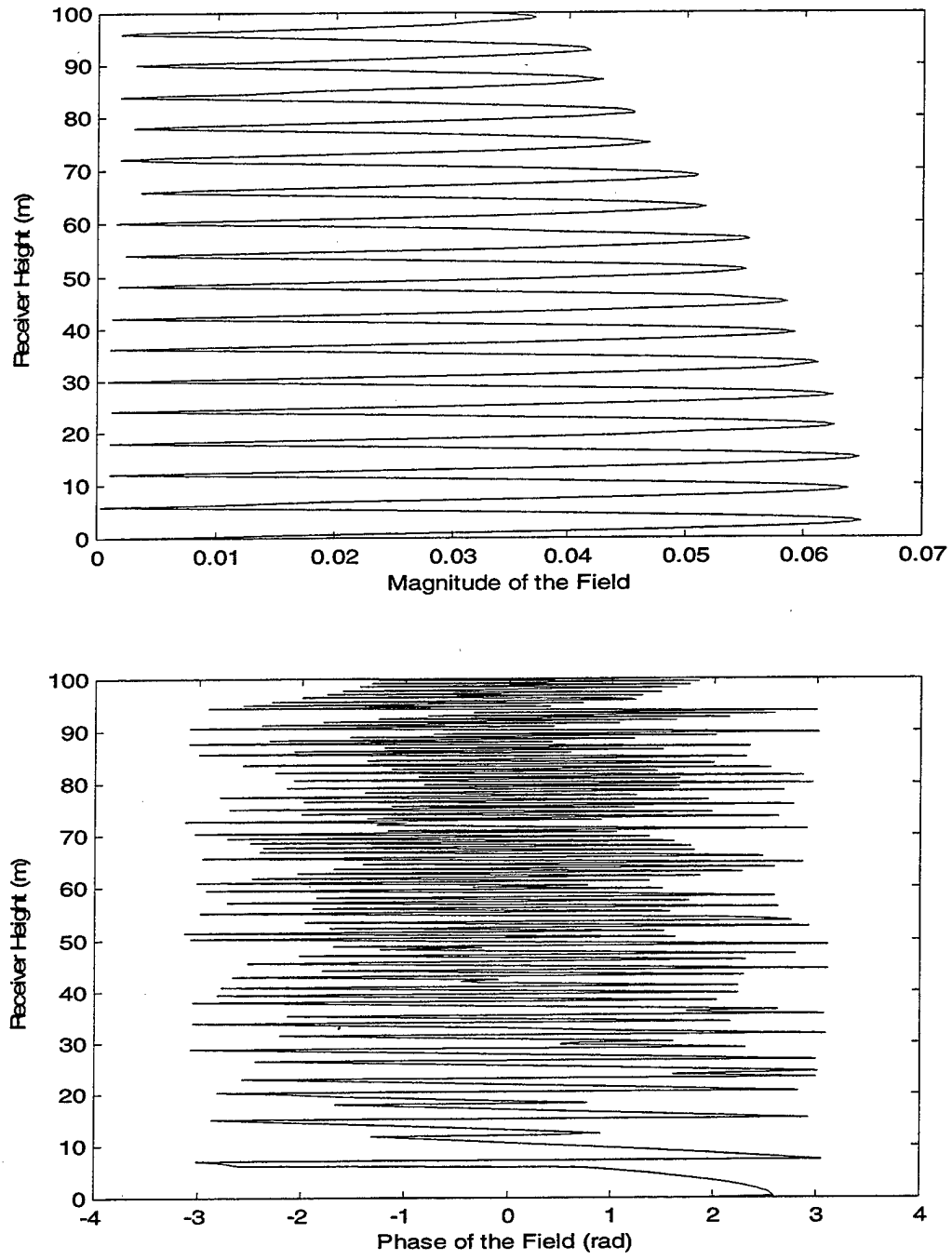

Figure 12: Magnitude and Phase of the Field at the End of the First Section for Case 2 of Flat Surface.

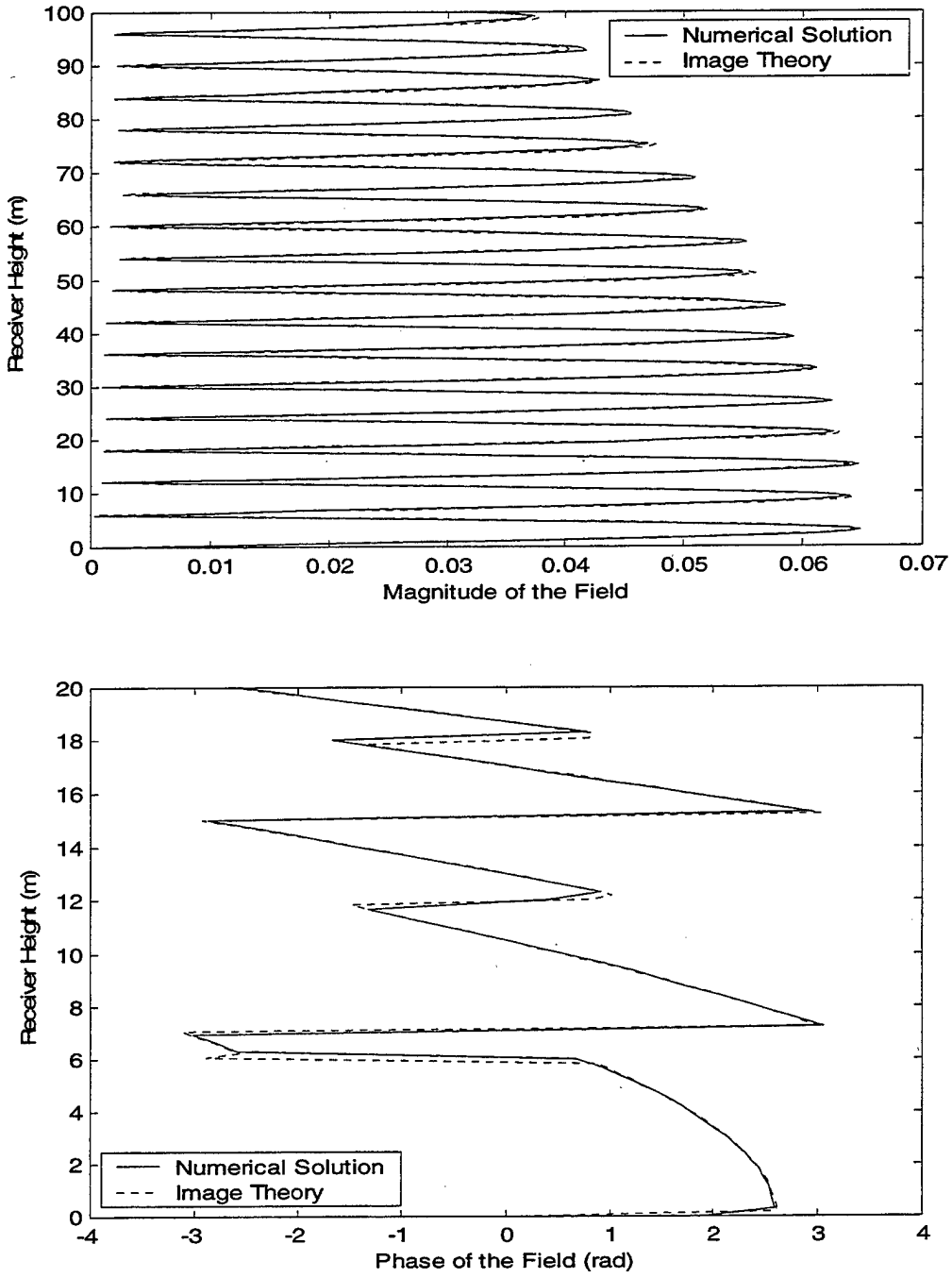

Figure 13: Magnitude and Phase of the Field at the End of the First Section for Case 2 of Flat Surface.

B. PROPAGATION OVER PEC KNIFE-EDGE

Consider an ideal absorbing knife-edge of height $h_p = 5$ meters on a conducting plane, as shown in Figure 14, where we have a = b = c = d = 50 m. The transmitter antenna height is 3 meters ($z_t = 3$) and it is located at point A. One wants to calculate the PF at a vertical line located at B, distant 200 m from the transmitter antenna.

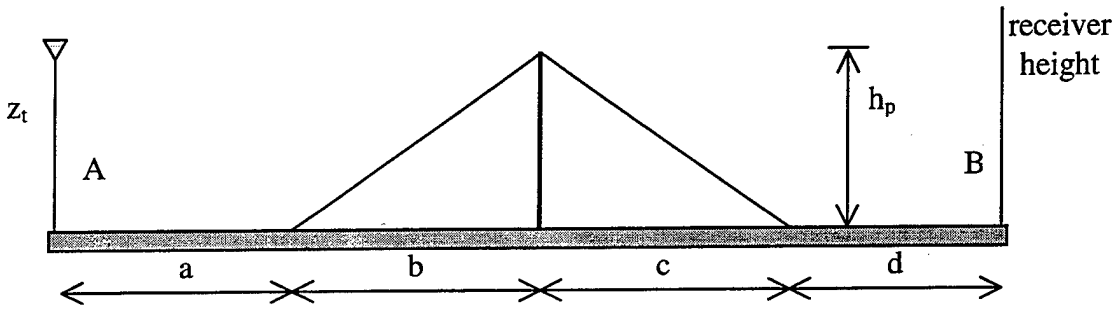

Figure 14: Perfectly Absorber Knife-Edge Between the Transmitter at A and a Vertical Line at B, Where the Propagation Factor is Being Evaluated. Both are over Perfectly Conducting Ground.

We compare our numerical solution with a four-ray model of knife-edge diffraction theory [Ref. 4]. In the parabolic equation computations we replace the knife-edge with a triangular hill having a base of 100 m (b = c = 50 m in Figure 14) and a peak height of 5 m. The numerical results are plotted in Figure 15. We notice that the total current and the incident current are the same for the first 50 m (corresponding to portion *a*), since we have flat surface for this part of the terrain. We notice a good agreement for low heights, since the four-ray model assumes large distances. If we now move both the triangular peak and the vertical line B to the right, making a = d = 150 m and b = c = 50

m on Figure 14 we have the numerical results shown in Figure 16. Moving the triangular peak and the vertical line B further to the right, making a = d = 250 m and b = c = 50 m on Figure 14, we have the results shown on Figure 17. Comparing Figure 15, Figure 16 and Figure 17 we notice progressively better agreement with increasing heights, since both models compared provide more accurate results for longer horizontal distances.

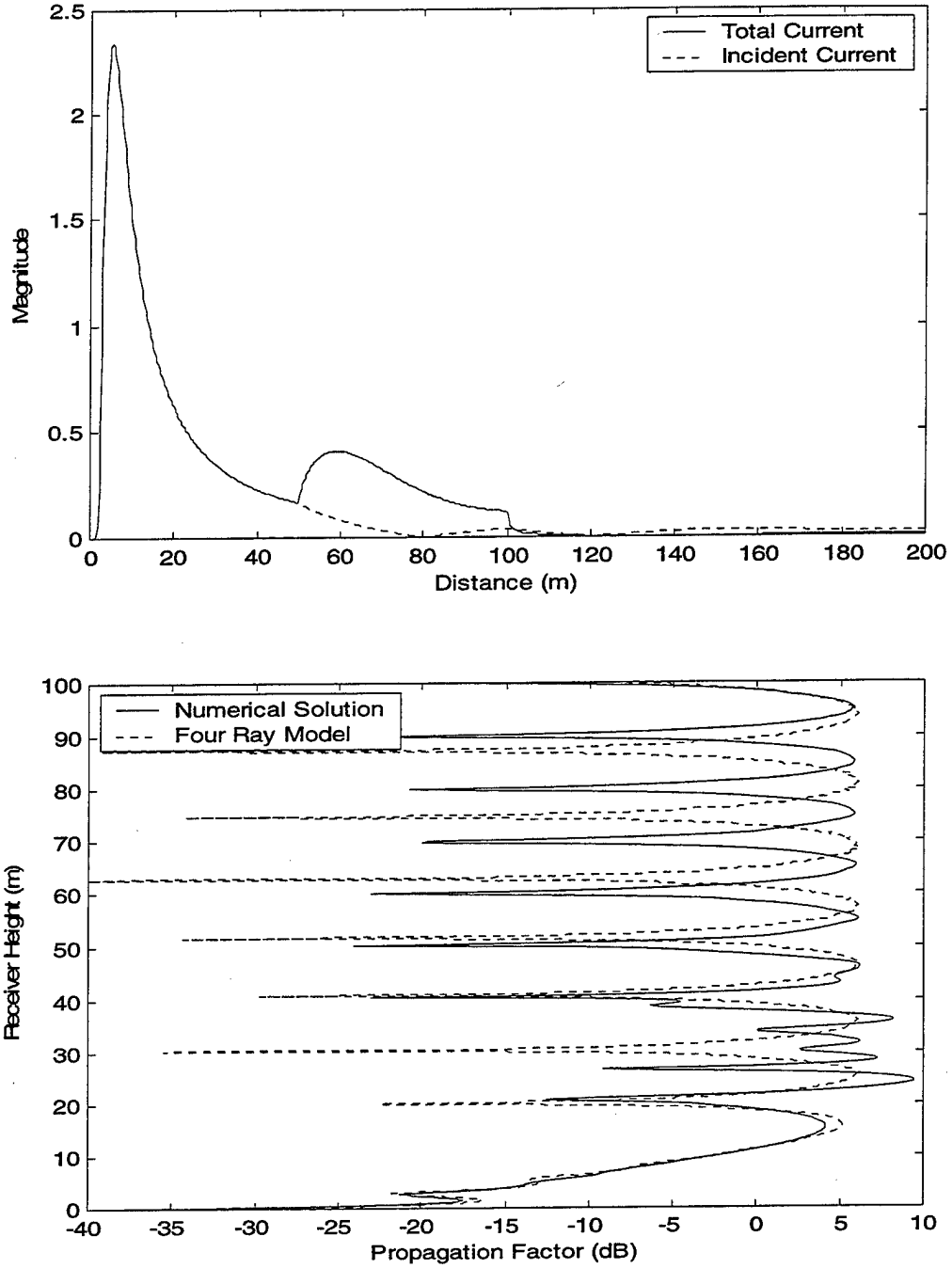

Figure 15: Total Current and Incident Current (Upper Figure) and Propagation Factor (Lower figure) for the Triangular Hill with a = b = c = d = 50 m, Peak Height = 5 m and Antenna Height = 3 m. Frequency = 1 GHz. Calculation in one section. $\Delta_x = \lambda$.

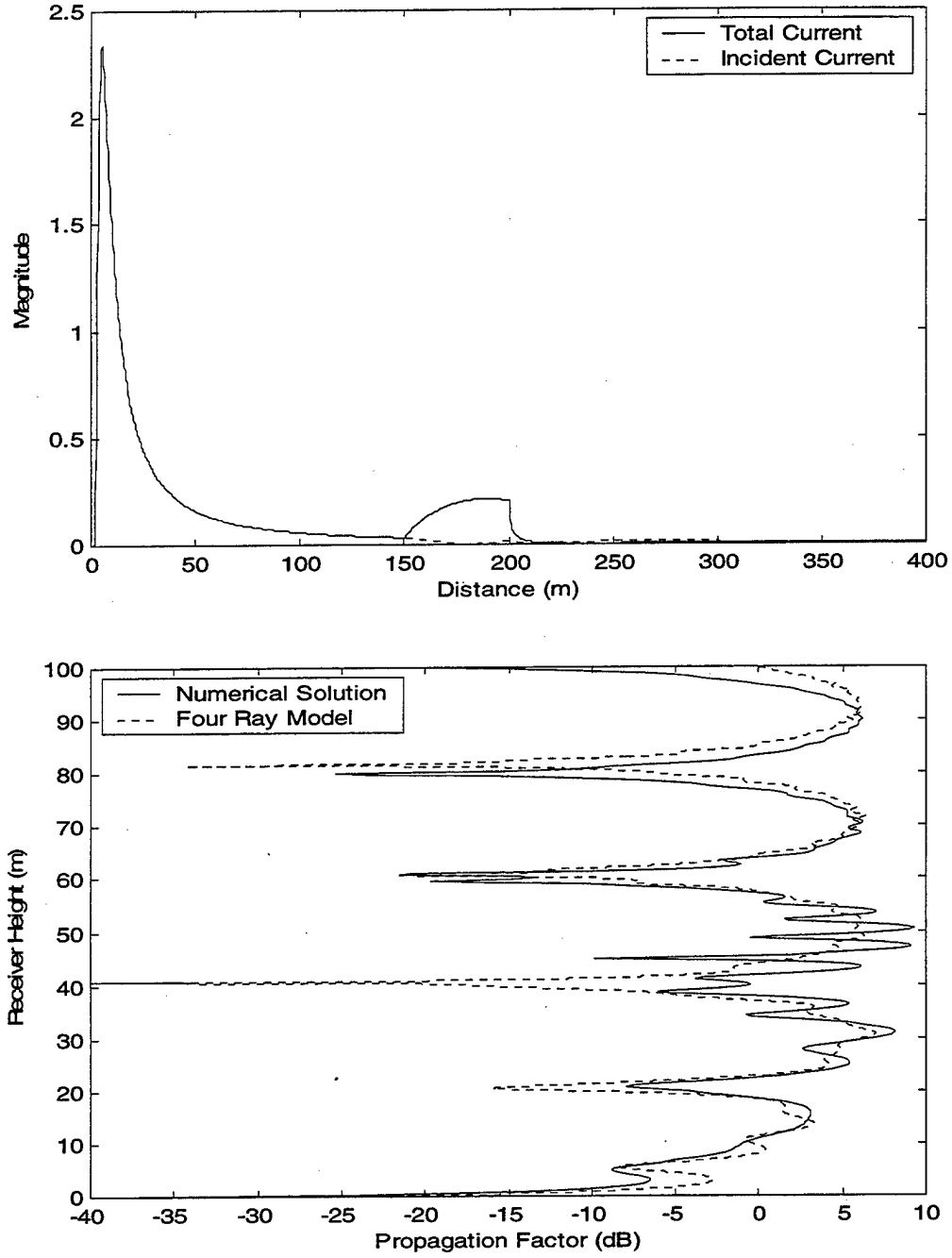

Figure 16: Total Current and Incident Current (Upper Figure) and Propagation Factor (Lower figure) for the Triangular Hill with a = d = 150 m, b = c = 50 m, Peak Height = 5 m and Antenna Height = 3 m. Frequency = 1 GHz. Calculation in one section. $\Delta_x = \lambda$.

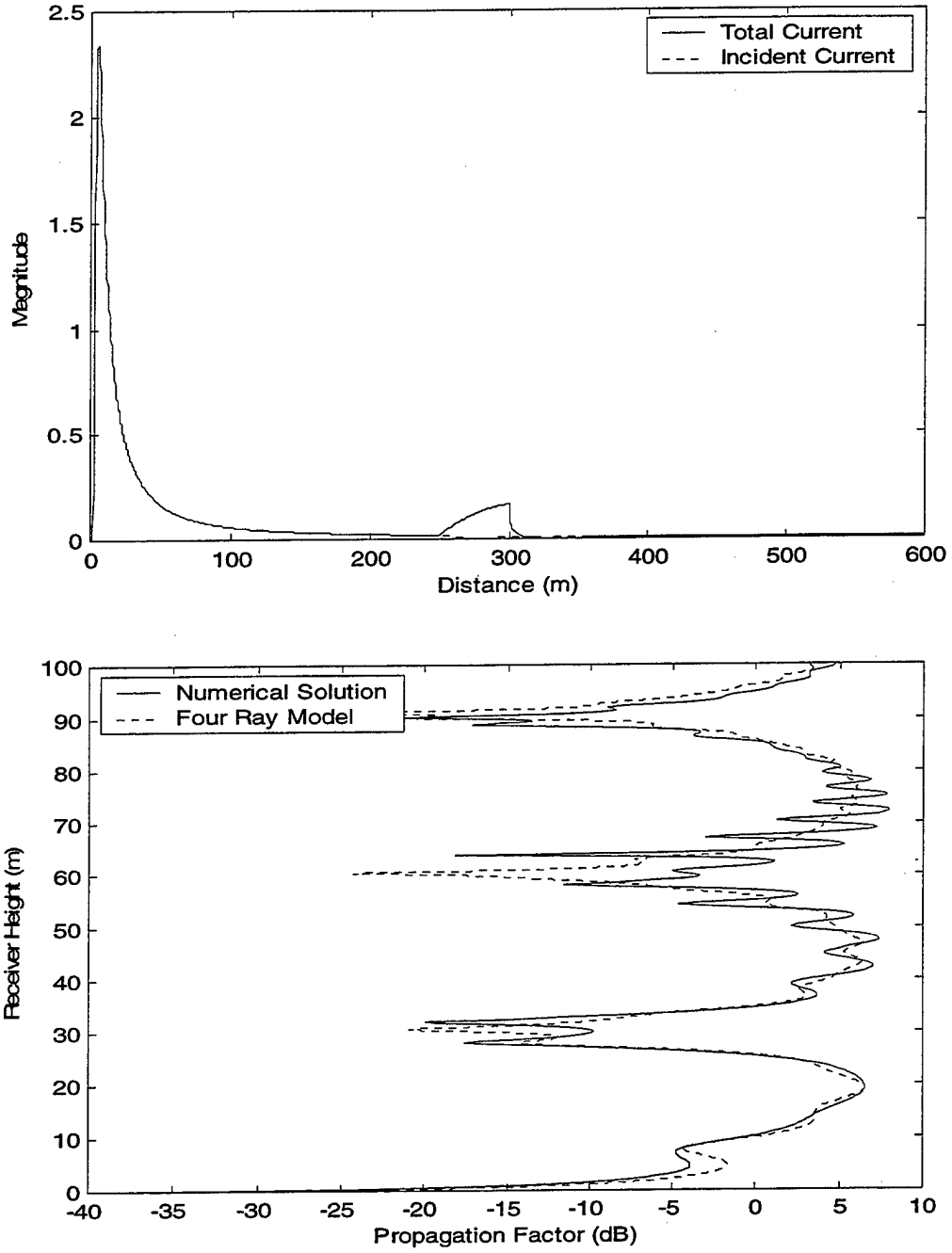

Figure 17: Total Current and Incident Current (Upper Figure) and Propagation Factor (Lower figure) for the Triangular Hill with a = d = 250 m, b = c = 50 m, Peak Height = 5 m and Antenna Height = 3 m. Frequency = 1 GHz. Calculation in one section. $\Delta_x = \lambda$.

C. PROPAGATION OVER A PEC SINUSOIDAL SURFACE AND EQUIVALENT IMPEDANCE DETERMINATION

Once we tested our solution for two important test cases, we can use the model for a rough surface. The only restriction we enforce is on the slope of the surface: as it increases, the waves are forced to travel in higher angles and the parabolic equation has an angular limitation of approximated 15° [Ref. 2]. In this section we will analyze the case of a sinusoidal surface. Initially we will evaluate the propagation factor and verify how fast we can march, i.e., how the results are sensitive to changes of the step size. Finally, we will determine the equivalent impedance for low grazing angles.

1. Propagation over a PEC sinusoidal surface

Consider a sinusoidal surface defined by

$$g(x)=\frac{A_{pp}}{2}\left(1-\cos\left(\frac{2\pi x}{T}+\theta\right)\right) \tag{3.3}$$

where A_{pp} is the peak to peak amplitude, x is the horizontal distance from the source, T is the period, θ an arbitrary phase and $g(x)$ the amplitude on that particular horizontal distance.

In Table 3.2 we have the relationship between the CPU time (Pentium MMX 266 MHz, *MATLAB* code) and the number of sections used in the calculation of the field over a total distance of 800 m on the sinusoidal surface with the following parameters: $A_{pp}=1\,\text{m}$, $T=30$ m, $\theta=0$. The distances d1, d2, d3 and so on are defined in Figure 18.

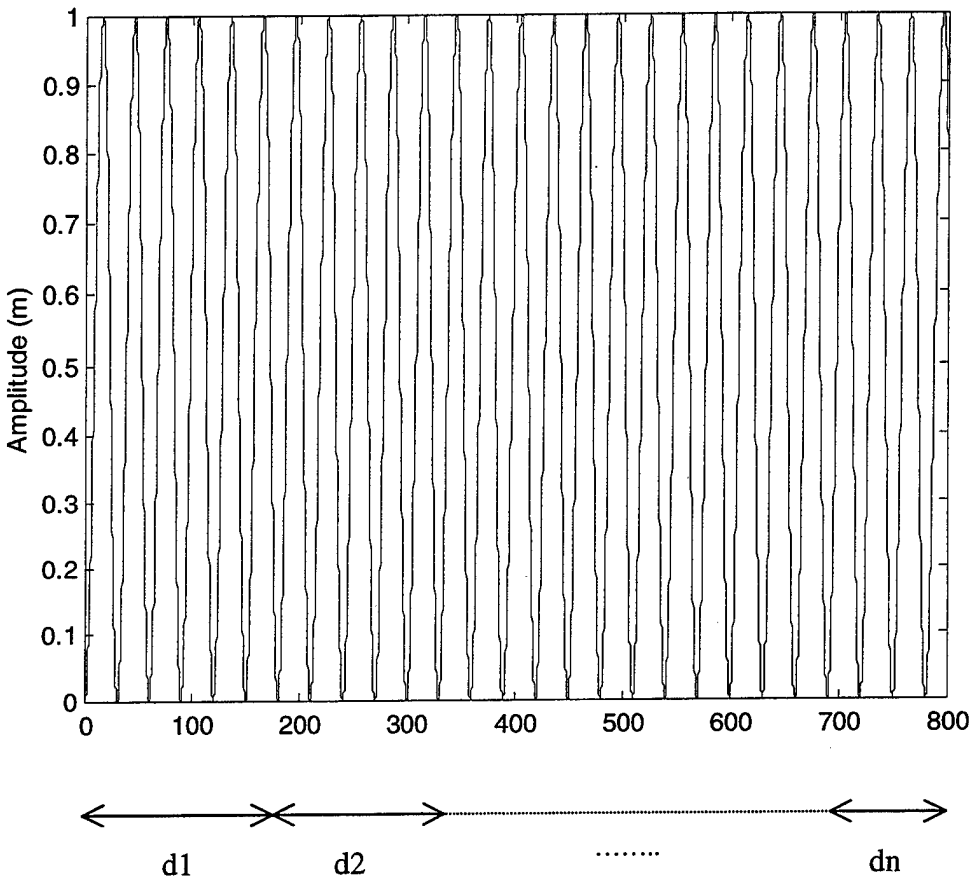

Figure 18: Sinusoidal Surface with Period = 30 m, Peak to Peak Amplitude = 1 m and Phase = 0°.

Case	N. of sec-tions	CPU time (hours)	% time	Section Size (m)								
				d1	d2	d3	d4	d5	d6	d7	d8	d9
1	1	5.0448	100	800	----	----	----	----	----	----	----	----
2	2	3.8496	76	600	200	----	----	----	----	----	----	----
3	2	3.5182	70	400	400	----	----	----	----	----	----	----
4	2	3.8698	77	200	600	----	----	----	----	----	----	----
5	3	2.8047	56	400	200	200	----	----	----	----	----	----
6	4	2.5889	51	400	200	100	100	----	----	----	----	----
7	5	2.3711	47	400	100	100	100	100	----	----	----	----
8	6	2.2611	45	400	80	80	80	80	80	----	----	----
9	7	2.1977	44	400	75	65	65	65	65	65	----	----
10	9	2.0920	41	400	50	50	50	50	50	50	50	50

Table 3.2: CPU time for Propagation over PEC Sinusoidal Surface

Figure 19 shows the incident current, the total current and the propagation factor when performing the calculation in one section. Figure 20, Figure 21 and Figure 22 show the incident current, the total current and the propagation factor when performing the calculation in two sections, gradually decreasing the length of the first section (d1) and increasing the length of the second section (d2). We notice that as we decrease the length of the first section and increase the length of the second section we have a disagreement among the results. Comparing cases 2 and 3 with case 1 the disagreement is not significant. However, case 4 and case 1 have completely different results.

Figure 23 shows the incident current, the total current and the propagation factor in three sections. Figure 24 shows the incident current, the total current and the propagation factor in nine sections.

Comparing Figure 19 and Figure 24, where we have the calculation in one section and nine sections respectively, we notice that the currents and the PF become very noisy for the last case. However, we have the computation time reduced to 41 % of the original one. In contrast to the case of flat surface, we observe that for propagation over rough surface we need to have many small sections to reach the point such that the computational time becomes minimum. This does not happen for the flat surface case because we had all g_{dn}'s equal to zero and we did not have to calculate the Fresnel integral when evaluating the I_n's (refer to Equation 2.19).

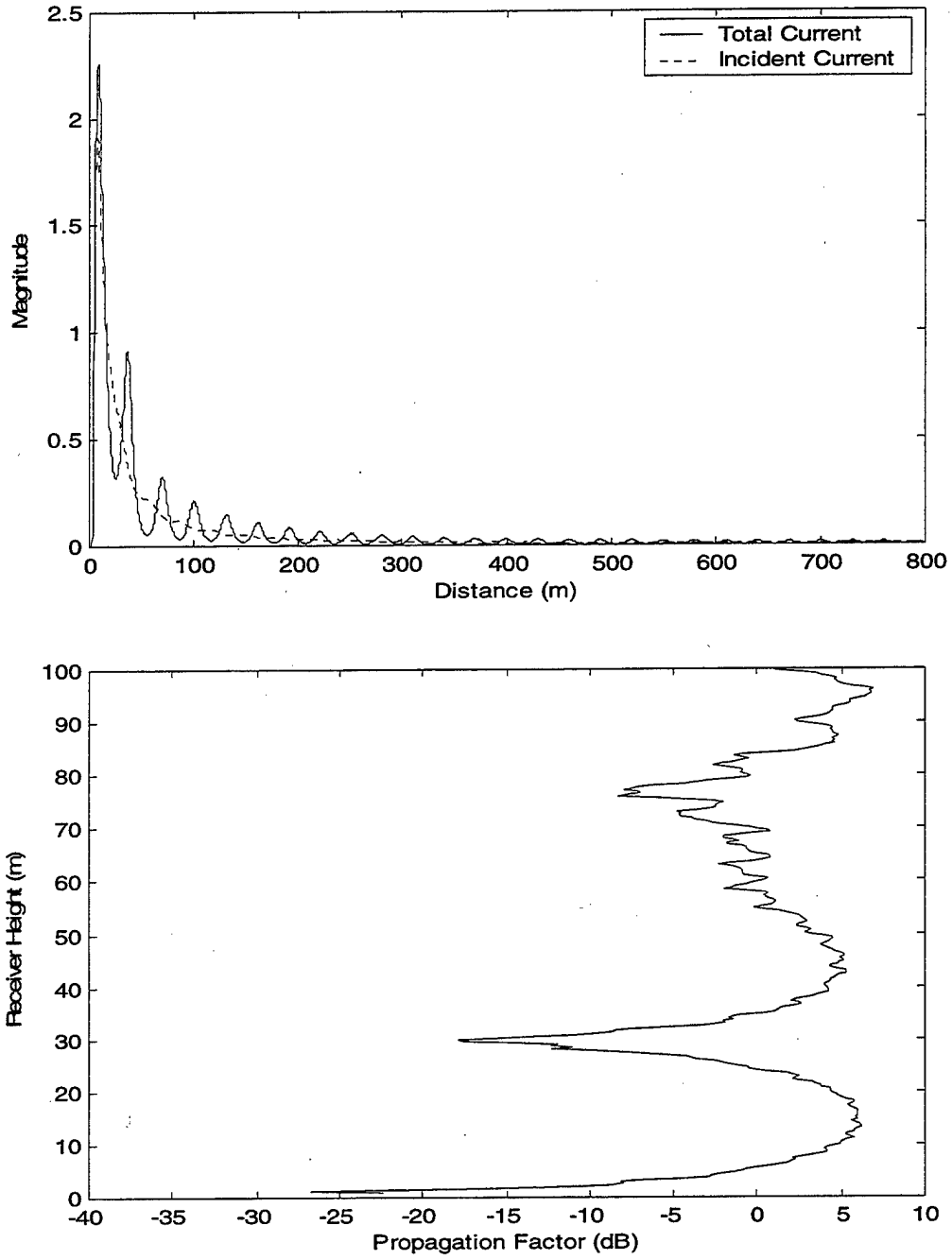

Figure 19: Total Current and Incident Current (Upper Figure) and Propagation Factor (Lower Figure) for the Case 1 of Sinusoidal Surface. Antenna Height = 5 m. Frequency = 1 GHz.

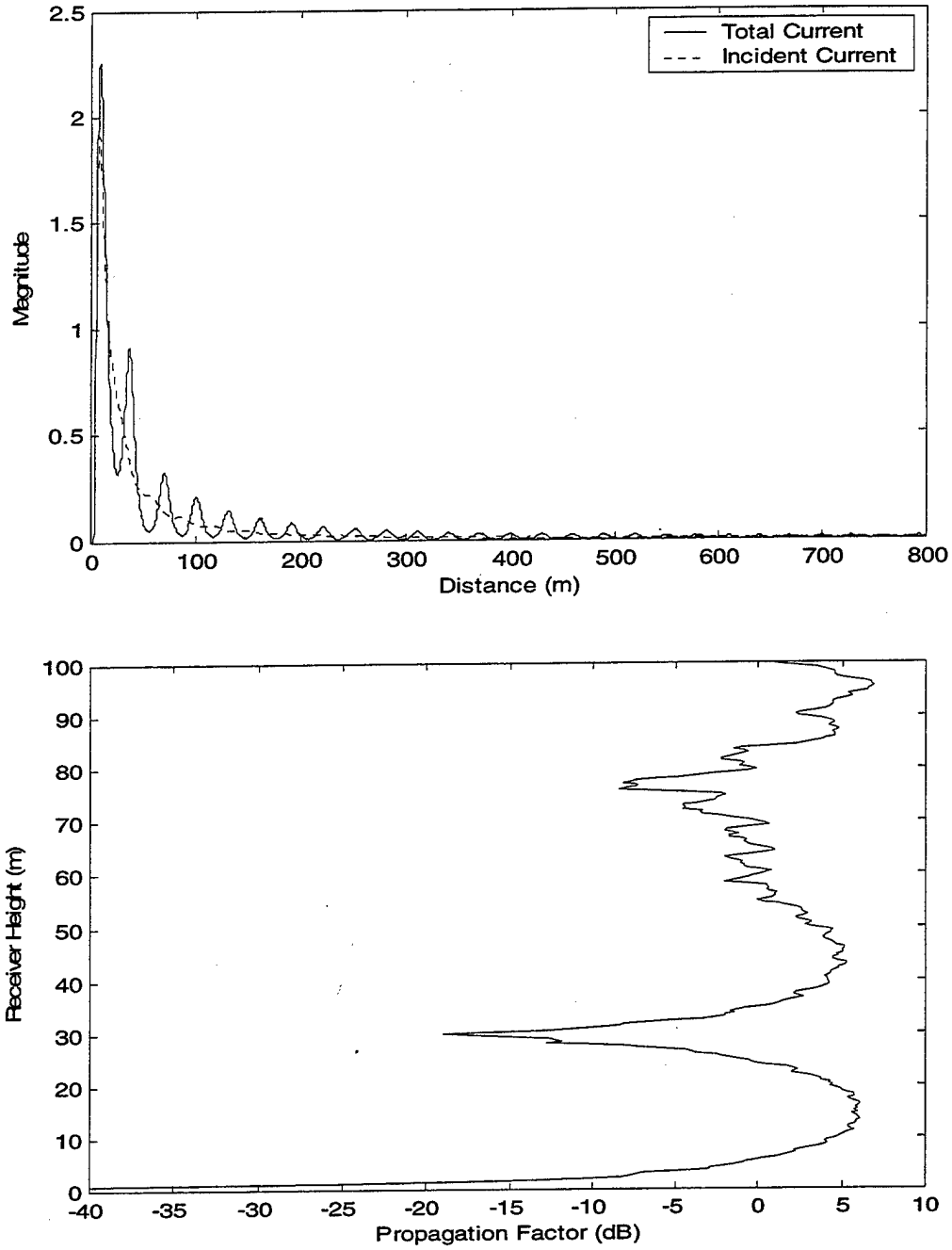

Figure 20: Total Current and Incident Current (Upper Figure) and Propagation Factor (Lower Figure) for the Case 2 of Sinusoidal Surface. Antenna Height = 5 m. Frequency = 1 GHz.

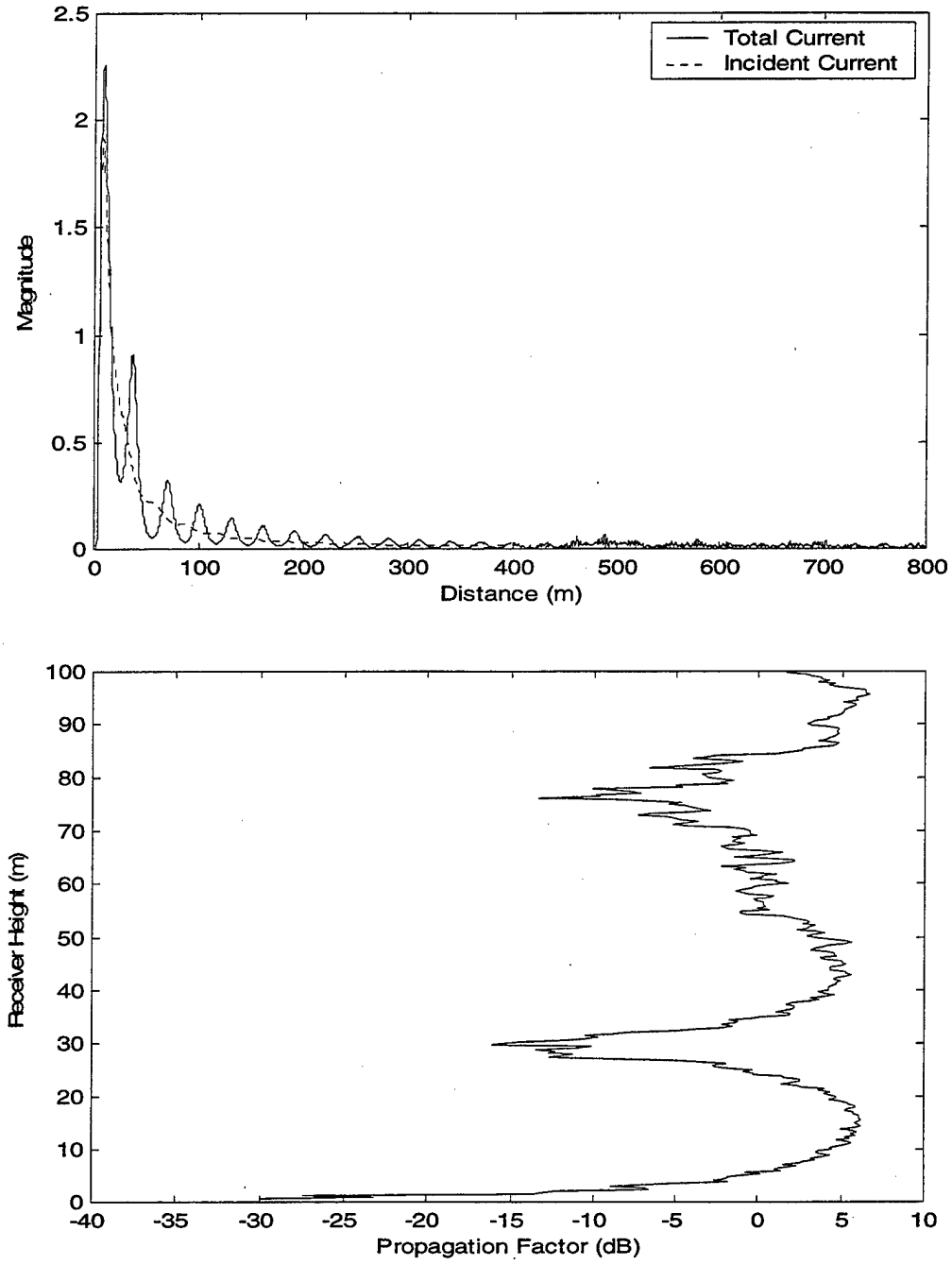

Figure 21: Total Current and Incident Current (Upper Figure) and Propagation Factor (Lower Figure) for the Case 3 of Sinusoidal Surface. Antenna Height = 5 m. Frequency = 1 GHz.

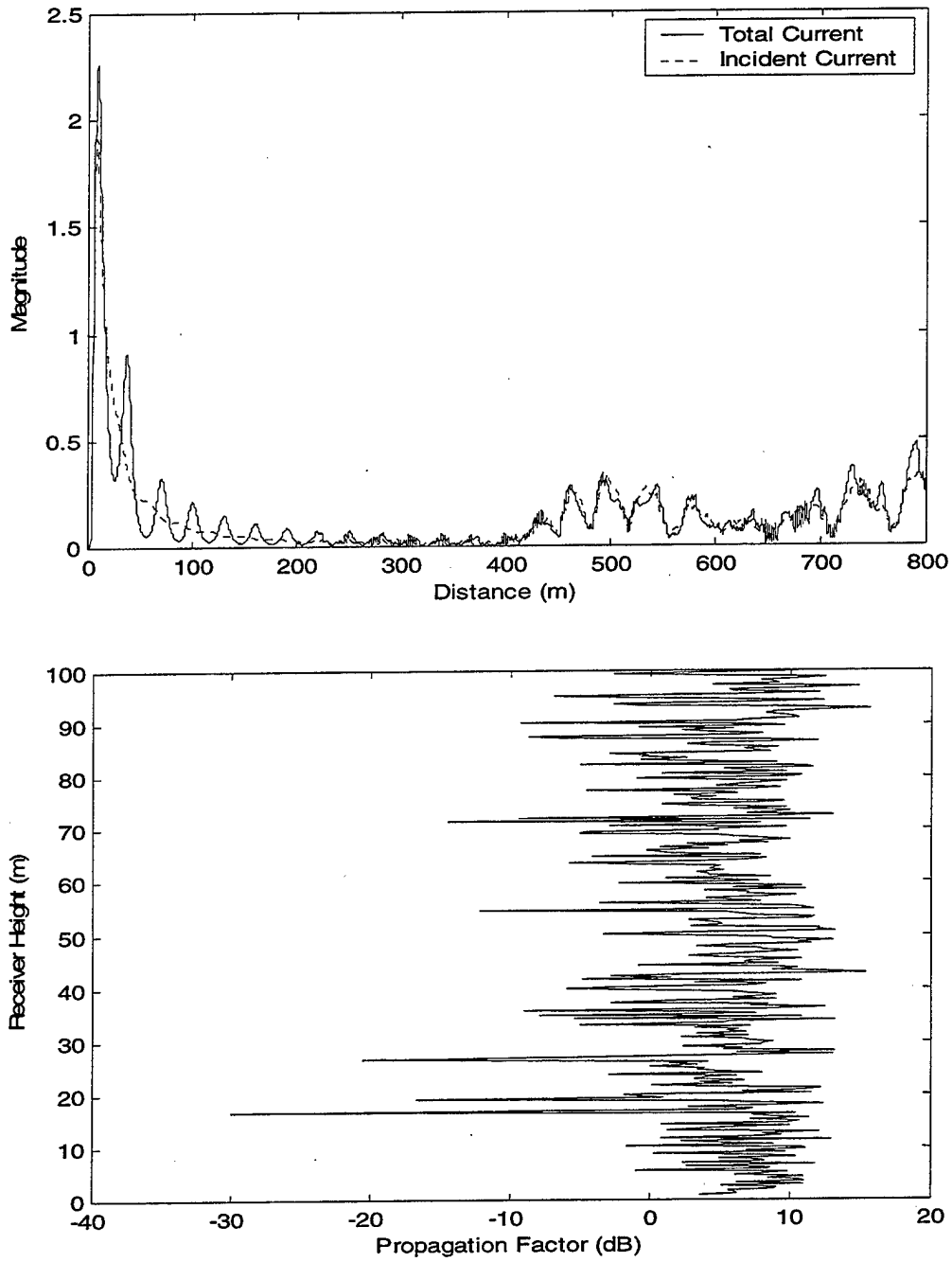

Figure 22: Total Current and Incident Current (Upper Figure) and Propagation Factor (Lower Figure) for the Case 4 of Sinusoidal Surface. Antenna Height = 5 m. Frequency = 1 GHz.

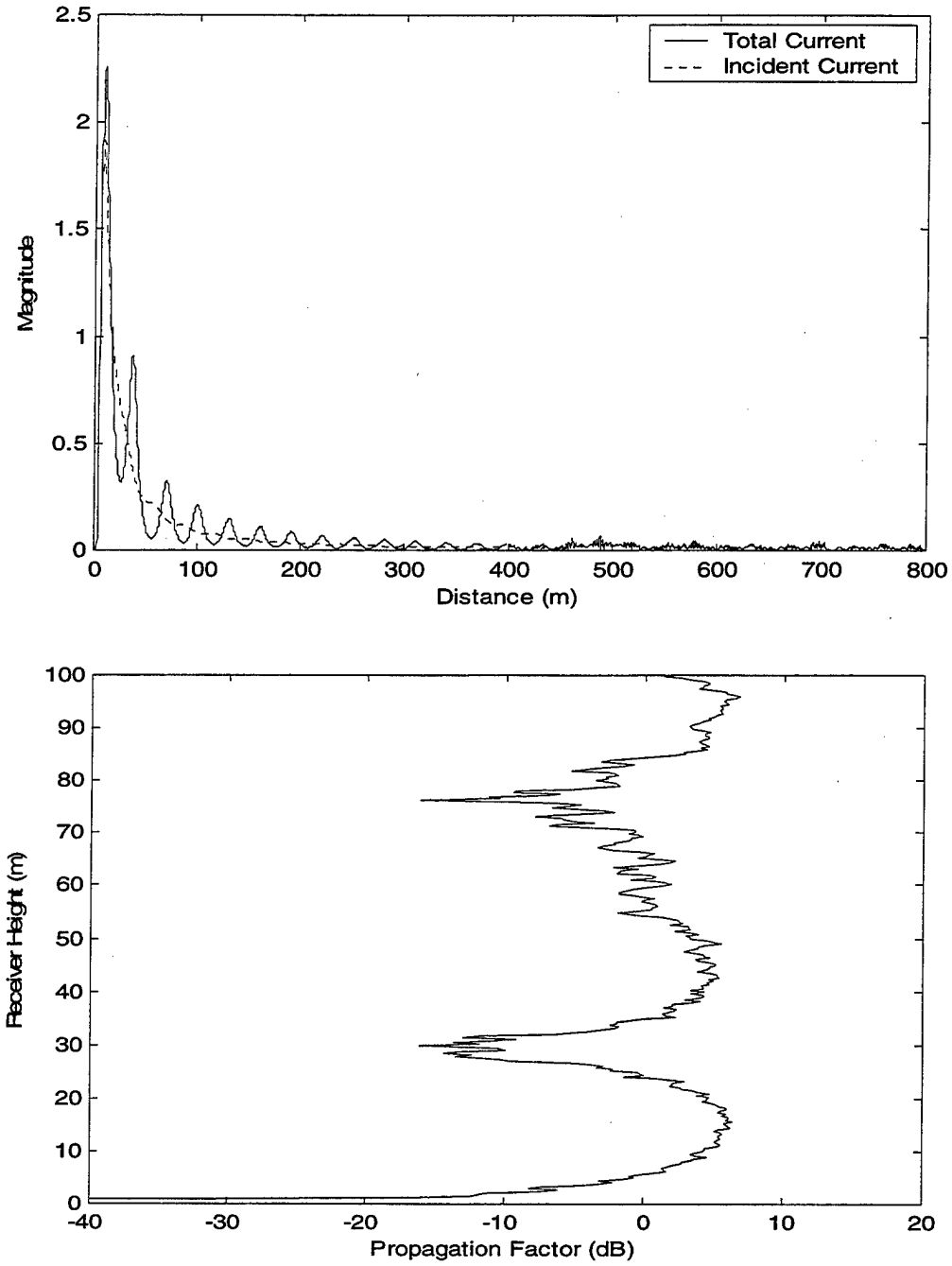

Figure 23: Total Current and Incident Current (Upper Figure) and Propagation Factor (Lower Figure) for the Case 5 of Sinusoidal Surface. Antenna Height = 5 m. Frequency = 1 GHz

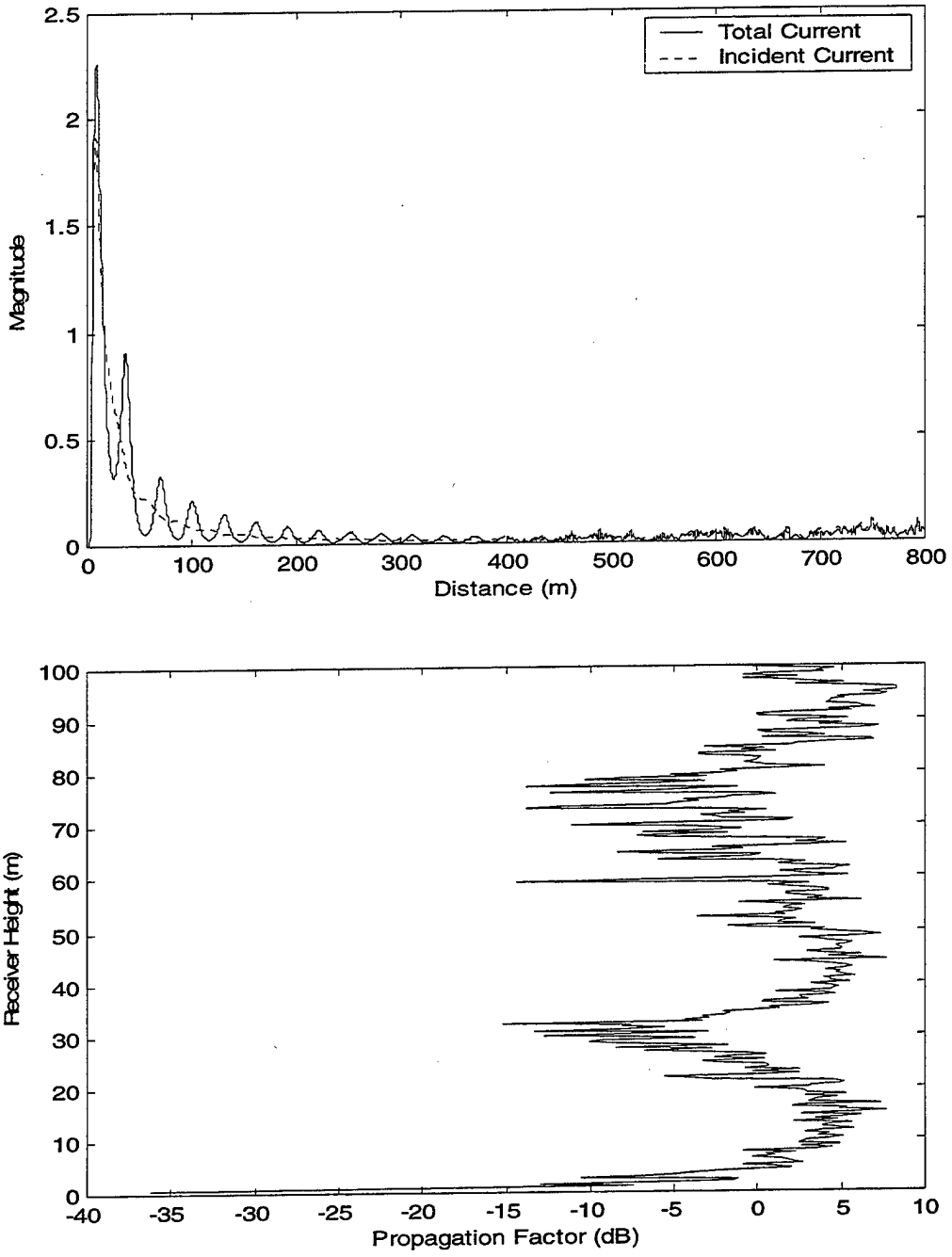

Figure 24: Total Current and Incident Current (Upper Figure) and Propagation Factor (Lower Figure) for the Case 10 of Sinusoidal Surface. Antenna Height = 5 m. Frequency = 1 GHz

2. Sensitivity to the step size, Δ_x, and to the standard deviation, σ_z, of the Gaussian source field

Consider propagation over a sinusoidal surface with the following parameters: $z_t = 5\,\text{m}$, $A_{pp} = 1\,\text{m}$, $T = 30\,\text{m}$, $x = 300\,\text{m}$, $\theta = 0^\circ$ and frequency of 1 GHz ($\lambda = 0.3\,\text{m}$). Figure 25, Figure 26, Figure 27, Figure 28, Figure 29 and Figure 30 shows the incident current, the total current and the PF for Δ_x equal to $\frac{\lambda}{2}$ $(0.15\,\text{m})$, λ $(0.3\,\text{m})$, 2λ $(0.6\,\text{m})$, 4λ $(1.2\,\text{m})$, 8λ $(2.4\,\text{m})$ and 16λ $(4.8\,\text{m})$ respectively and the source field with $\sigma_z = 0.1$. Figure 31, Figure 32, Figure 33, Figure 34, Figure 35 and Figure 36 shows the incident current, the total current and the PF for Δ_x equal to $\frac{\lambda}{2}$ $(0.15\,\text{m})$, λ $(0.3\,\text{m})$, 2λ $(0.6\,\text{m})$, 4λ $(1.2\,\text{m})$, 8λ $(2.4\,\text{m})$ and 16λ $(4.8\,\text{m})$ respectively and the source field with $\sigma_z = 0.4$.

We notice that for $\sigma_z = 0.1$ we have good results for both the total current and the PF for Δ_x up to 2λ. For $\sigma_z = 0.4$ we have good results for the total current for Δ_x up to 16λ, although even for small Δ_x $(\lambda/2)$ we have problems with the PF for high heights. This happens because the free-space field becomes very small for those heights due to the Gaussian distribution and numerical errors are introduced. In Figure 37 we notice that for $\sigma_z = 0.1\,\text{m}$ the free space field has almost constant magnitude at the receiver location, while for $\sigma_z = 0.4\,\text{m}$ the field magnitude decays as we go higher. The field becomes too small for high heights and numerical errors are introduced when computing the PF.

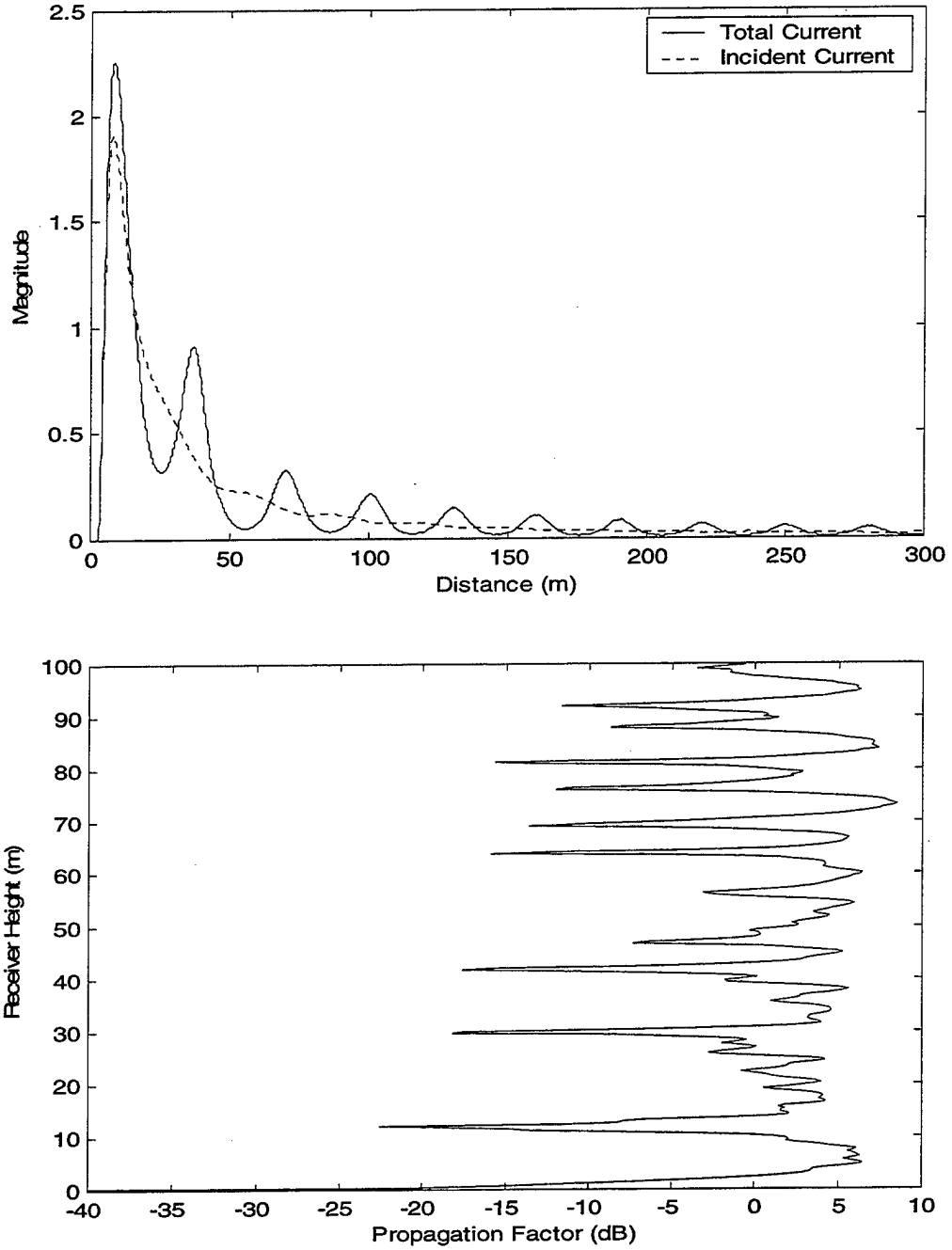

Figure 25: Total Current and Incident Current (Upper Figure) and Propagation Factor (Lower Figure) for Propagation over Sinusoidal Surface. $\Delta_x = \frac{\lambda}{2}$, $\sigma_z = \frac{\lambda}{3}$

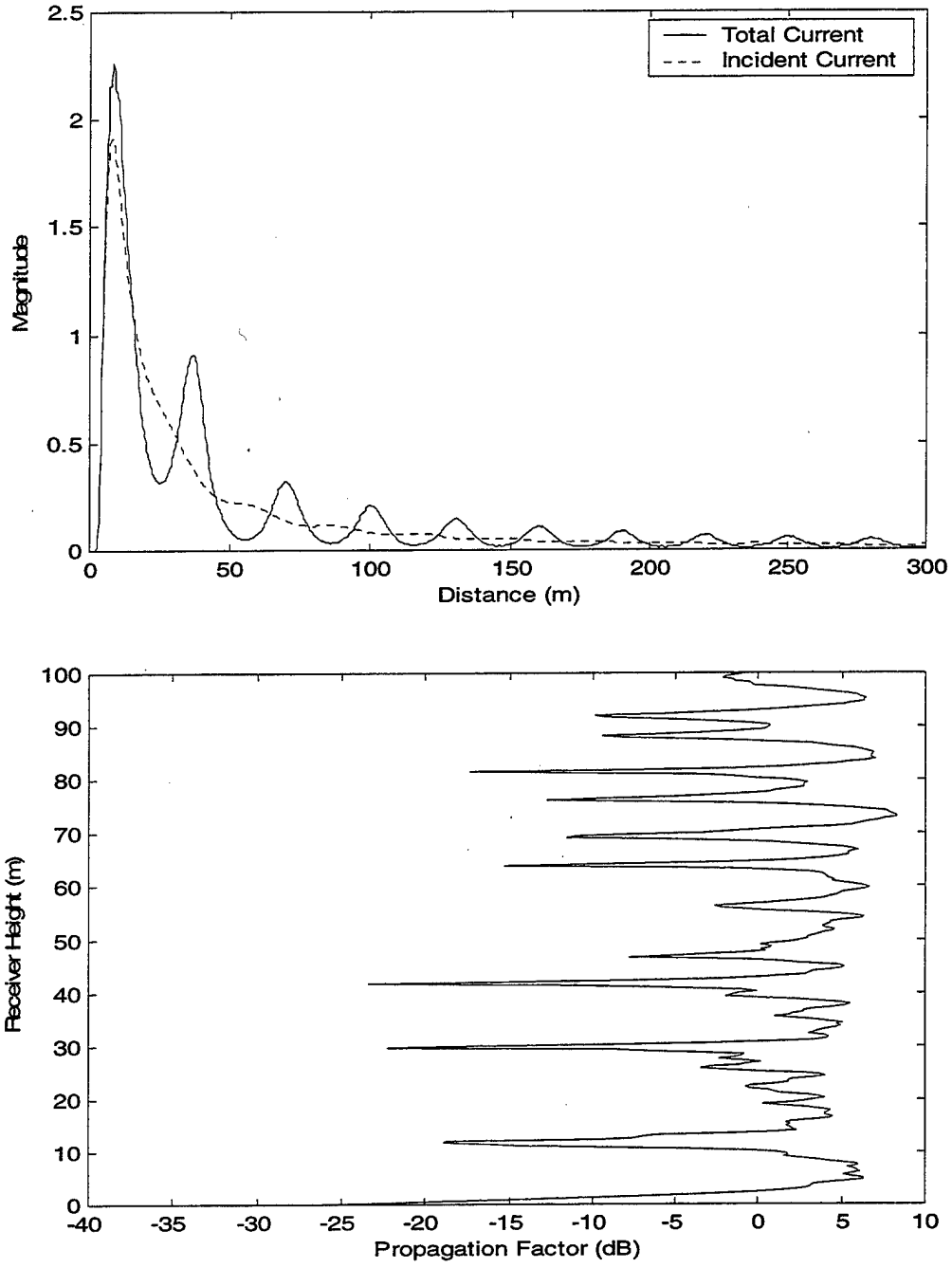

Figure 26: Total Current and Incident Current (Upper Figure) and Propagation Factor (Lower Figure) for Propagation over Sinusoidal Surface. $\Delta_x = \lambda$, $\sigma_z = \frac{\lambda}{3}$

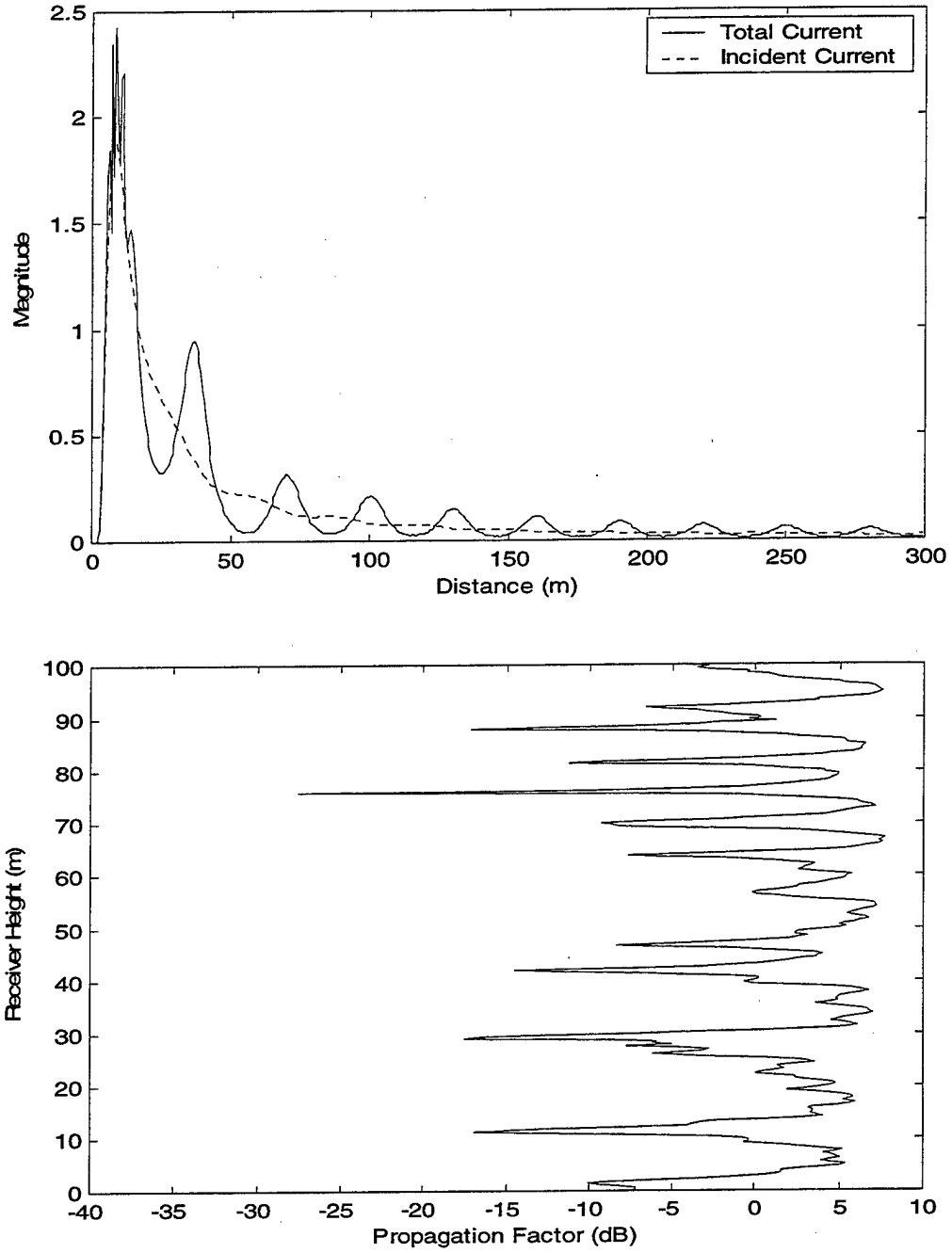

Figure 27: Total Current and Incident Current (Upper Figure) and Propagation Factor (Lower Figure) for Propagation over Sinusoidal Surface. $\Delta_x = 2\lambda$, $\sigma_z = \frac{\lambda}{3}$

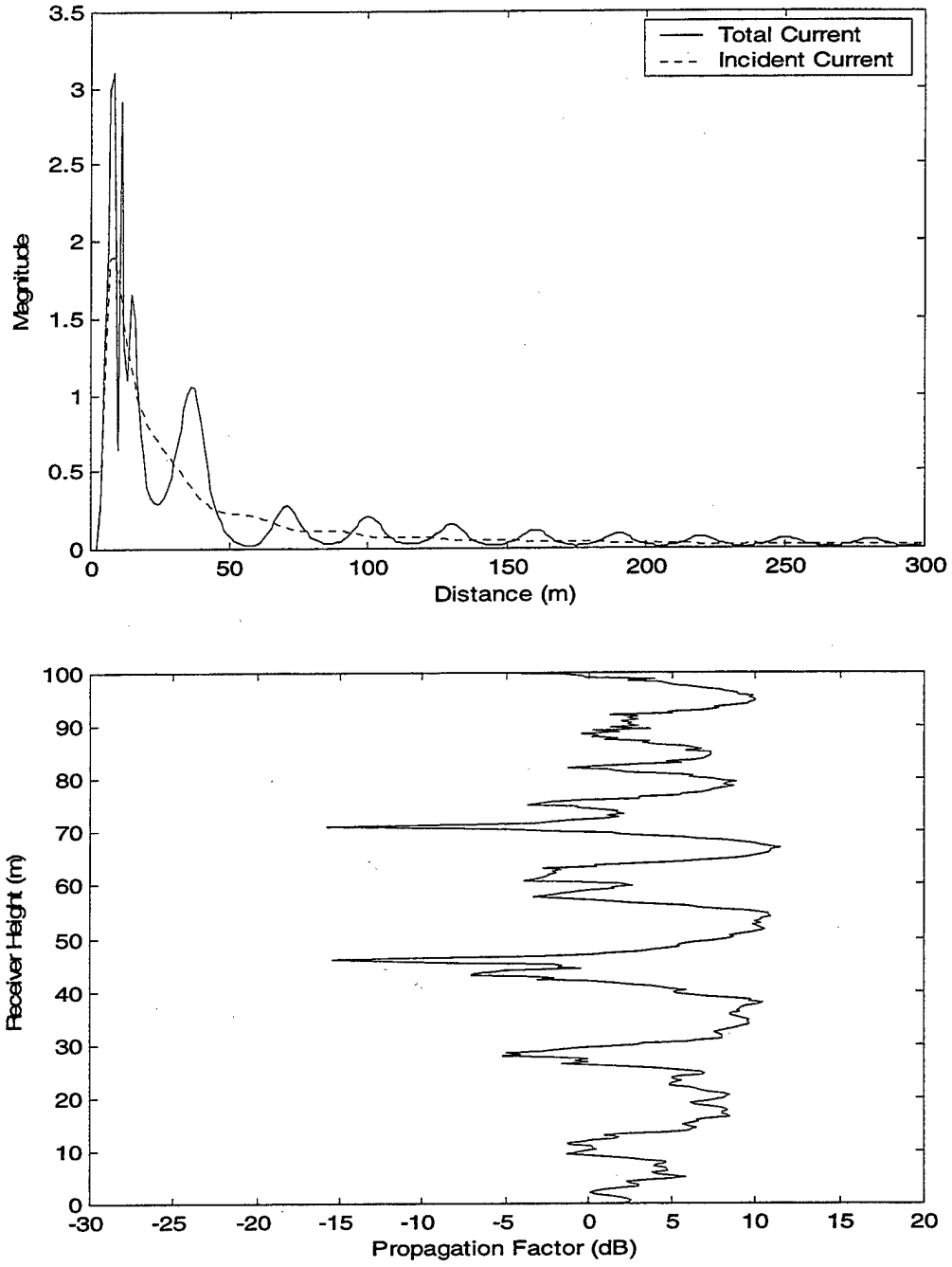

Figure 28: Total Current and Incident Current (Upper Figure) and Propagation Factor (Lower Figure) for Propagation over Sinusoidal Surface. $\Delta_x = 4\lambda$, $\sigma_z = \frac{\lambda}{3}$

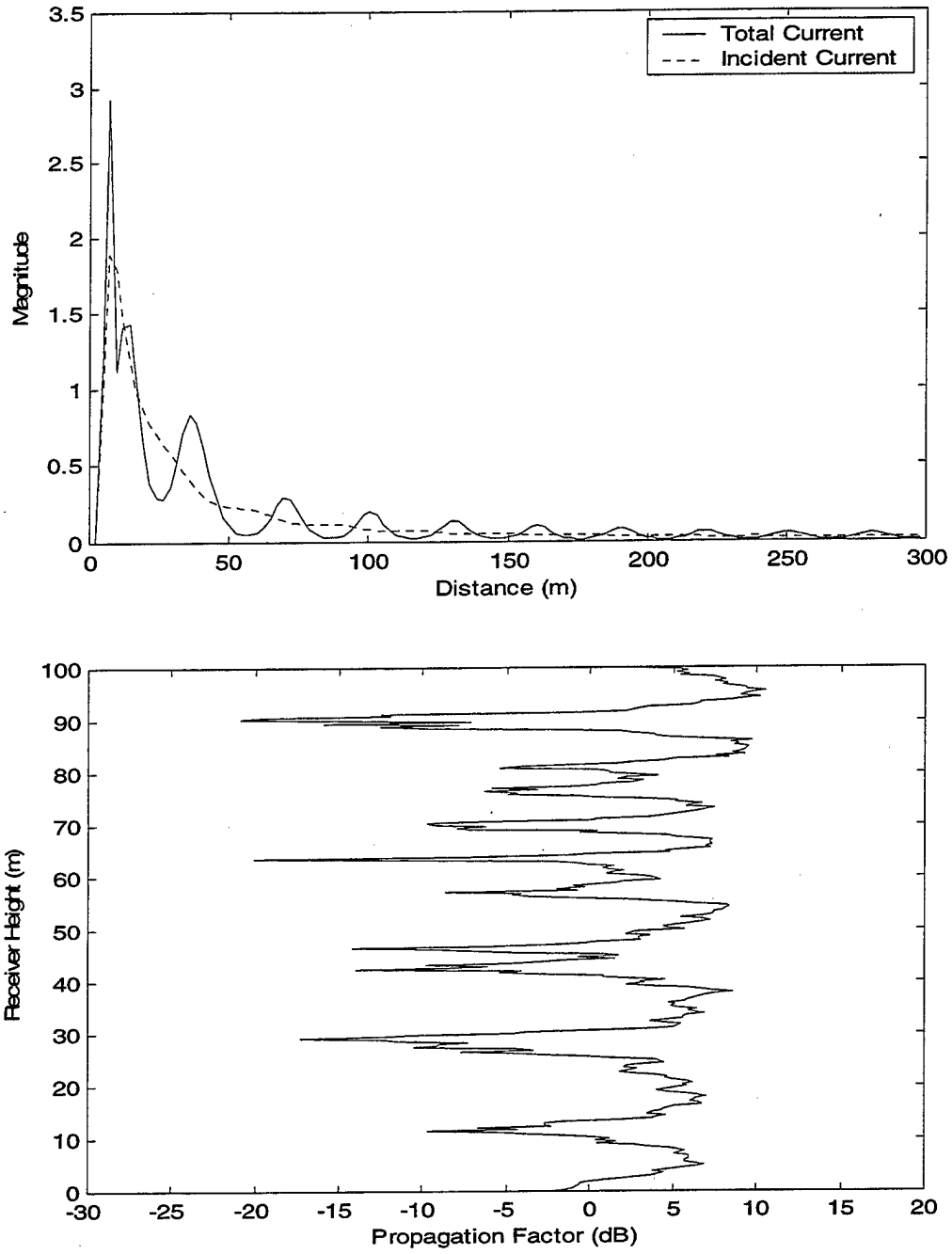

Figure 29: Total Current and Incident Current (Upper Figure) and Propagation Factor (Lower Figure) for Propagation over Sinusoidal Surface. $\Delta_x = 8\lambda$, $\sigma_z = \frac{\lambda}{3}$

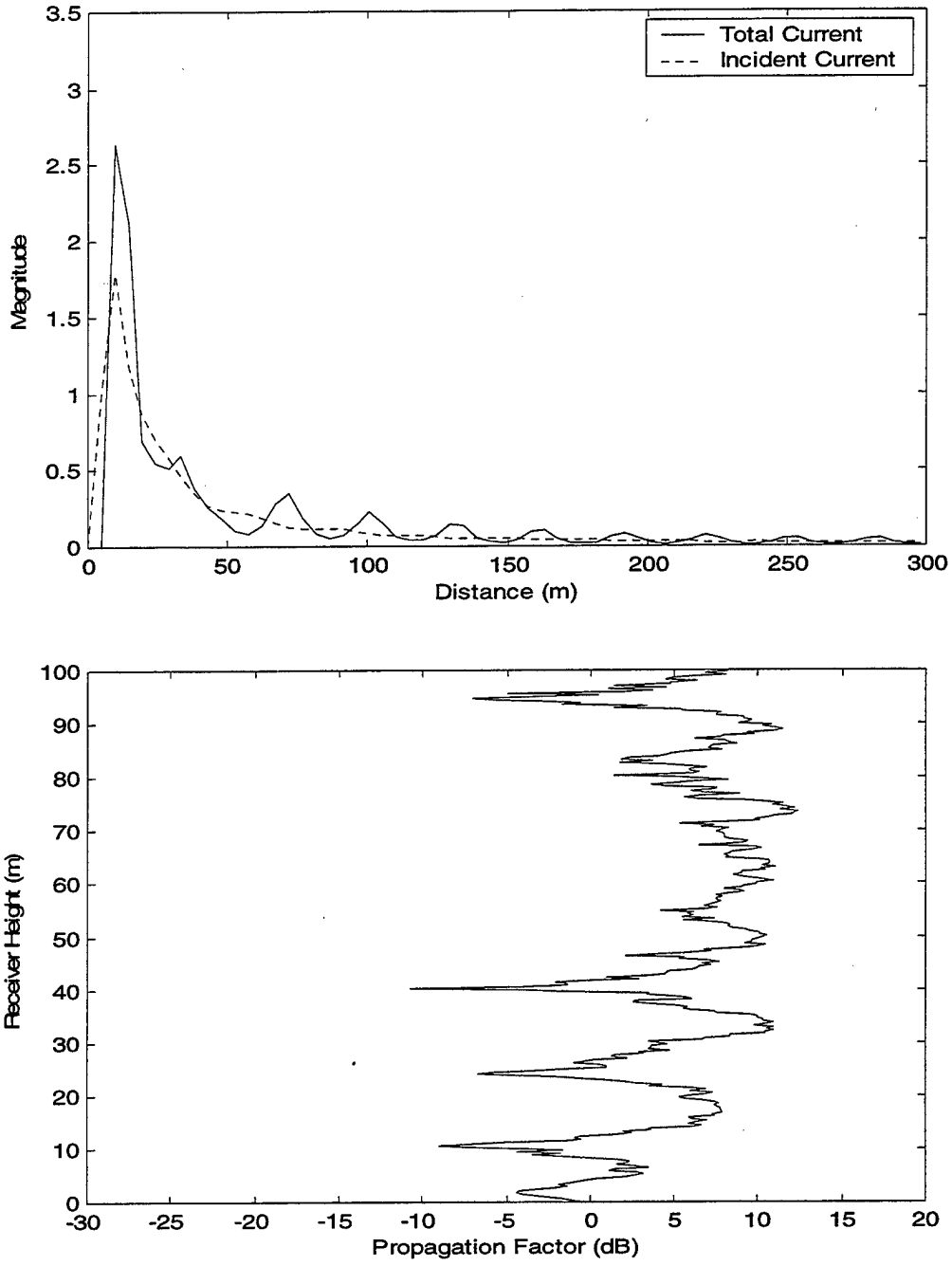

Figure 30: Total Current and Incident Current (Upper Figure) and Propagation Factor (Lower Figure) for Propagation over Sinusoidal Surface. $\Delta_x = 16\lambda$, $\sigma_z = \frac{\lambda}{3}$

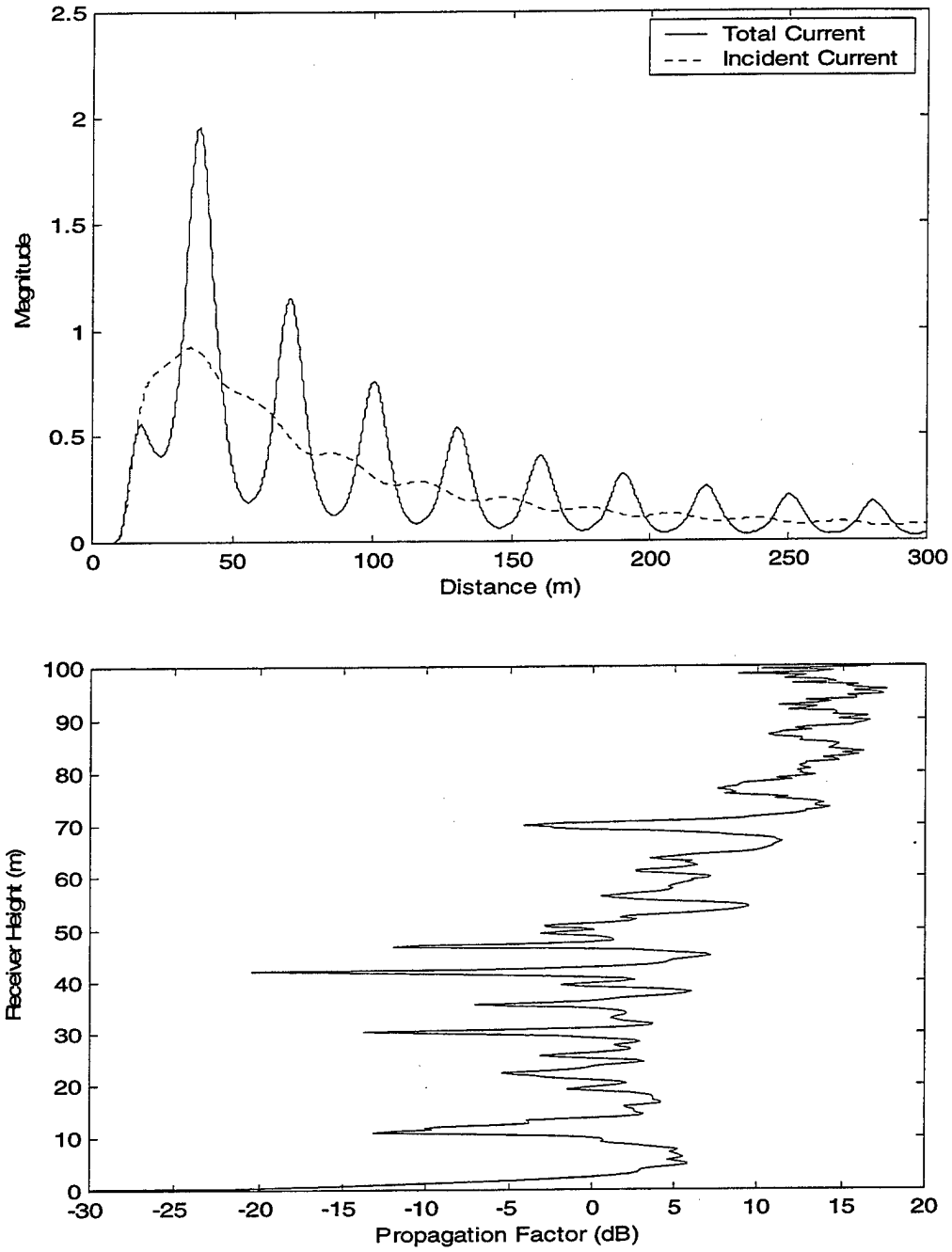

Figure 31: Total Current and Incident Current (Upper Figure) and Propagation Factor (Lower Figure) for Propagation over Sinusoidal Surface. $\Delta_x = \frac{\lambda}{2}$, $\sigma_z = \frac{4\lambda}{3}$

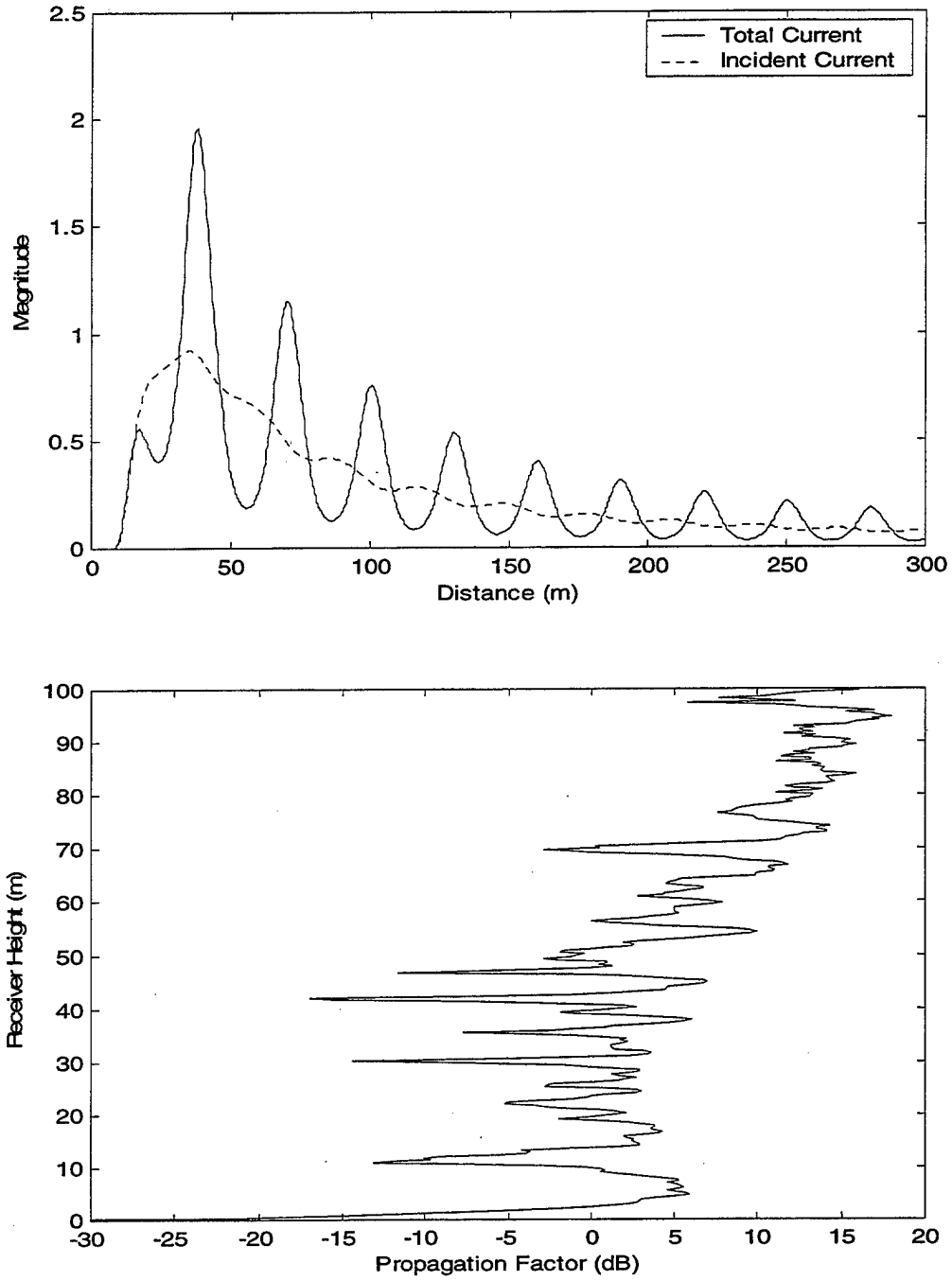

Figure 32: Total Current and Incident Current (Upper Figure) and Propagation Factor (Lower Figure) for Propagation over Sinusoidal Surface. $\Delta_x = \lambda$, $\sigma_z = \frac{4\lambda}{3}$

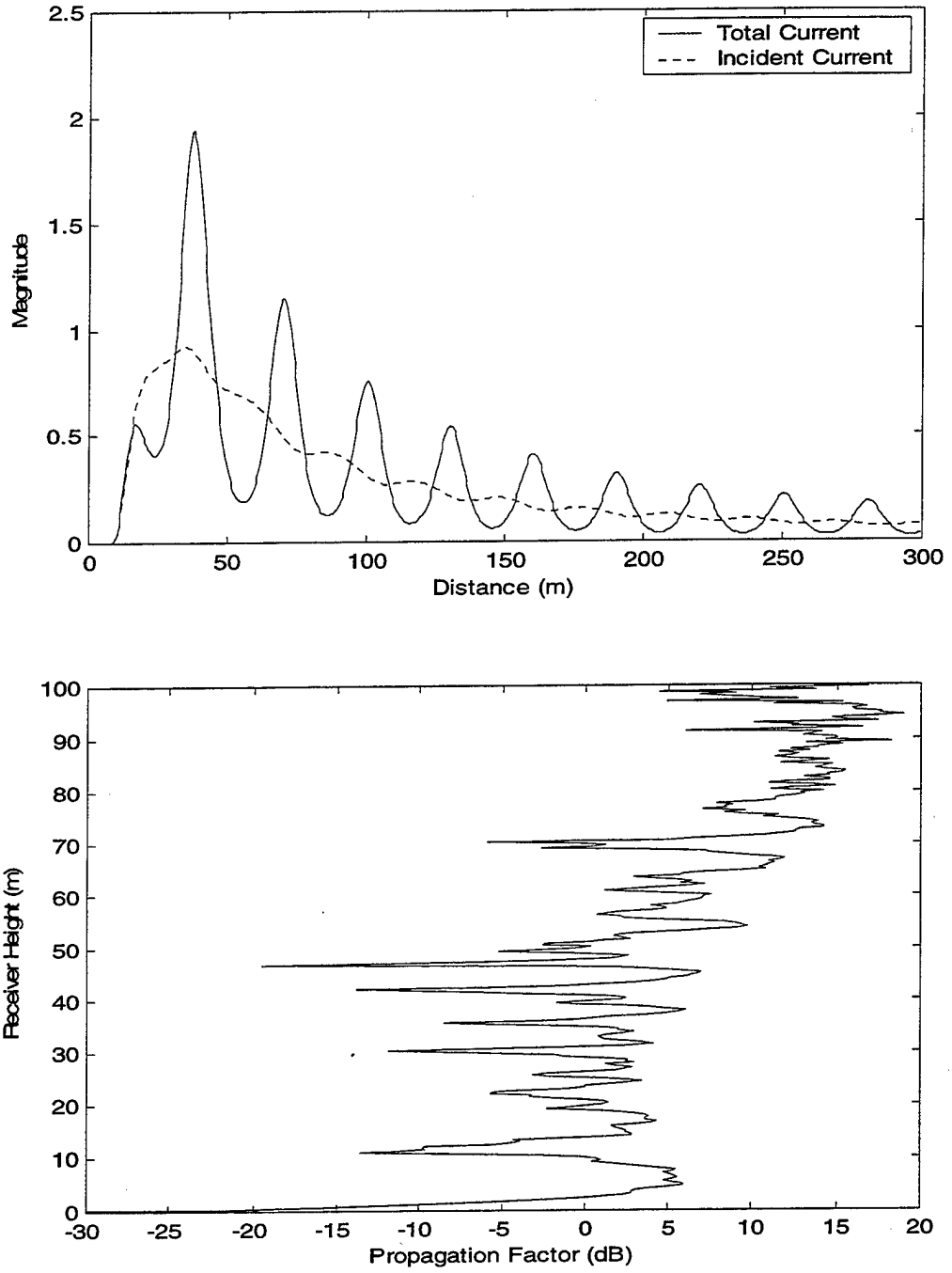

Figure 33: Total Current and Incident Current (Upper Figure) and Propagation Factor (Lower Figure) for Propagation over Sinusoidal Surface. $\Delta_x = 2\lambda$, $\sigma_z = \frac{4\lambda}{3}$

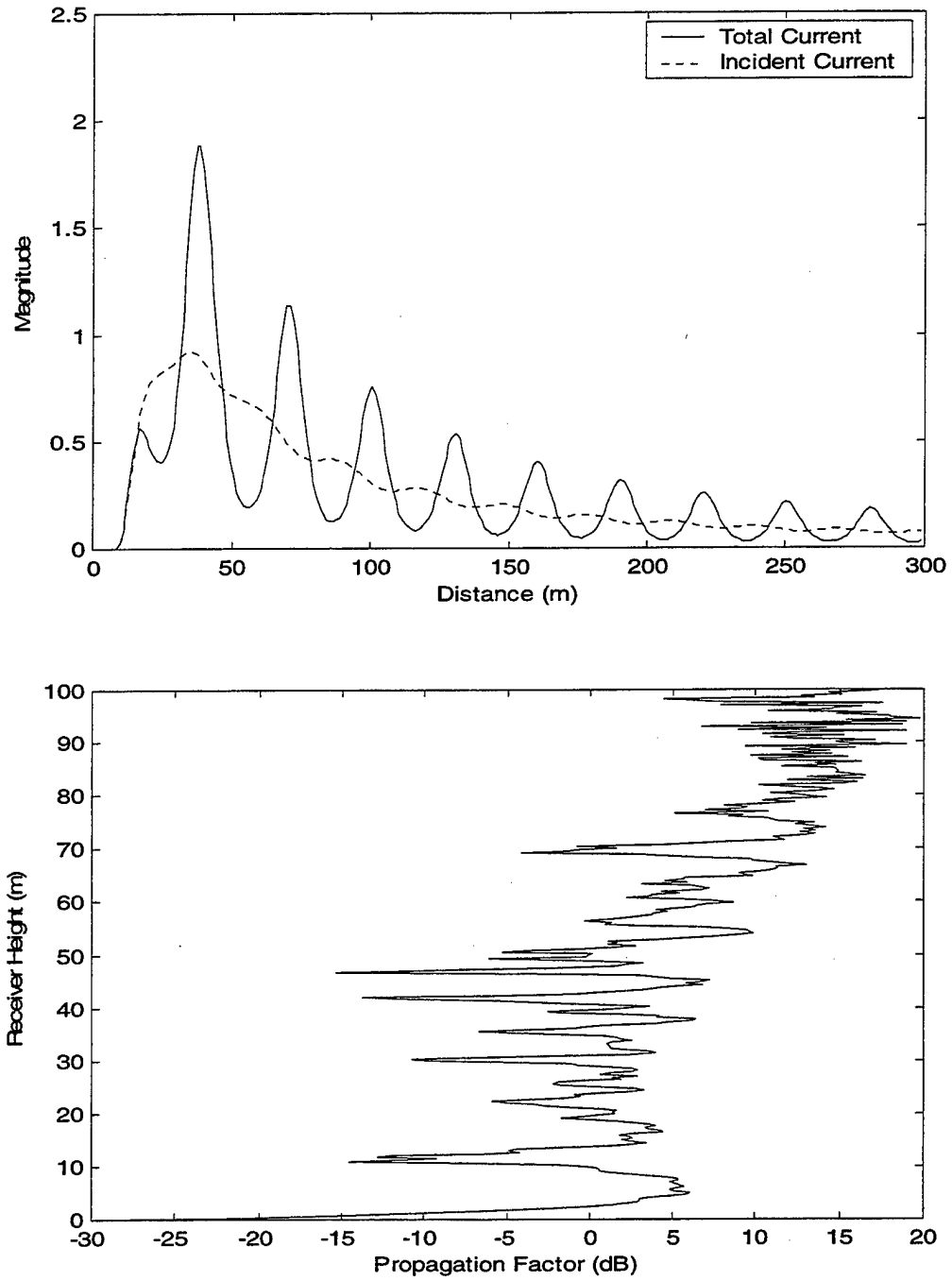

Figure 34: Total Current and Incident Current (Upper Figure) and Propagation Factor (Lower Figure) for Propagation over Sinusoidal Surface. $\Delta_x = 4\lambda$, $\sigma_z = \frac{4\lambda}{3}$

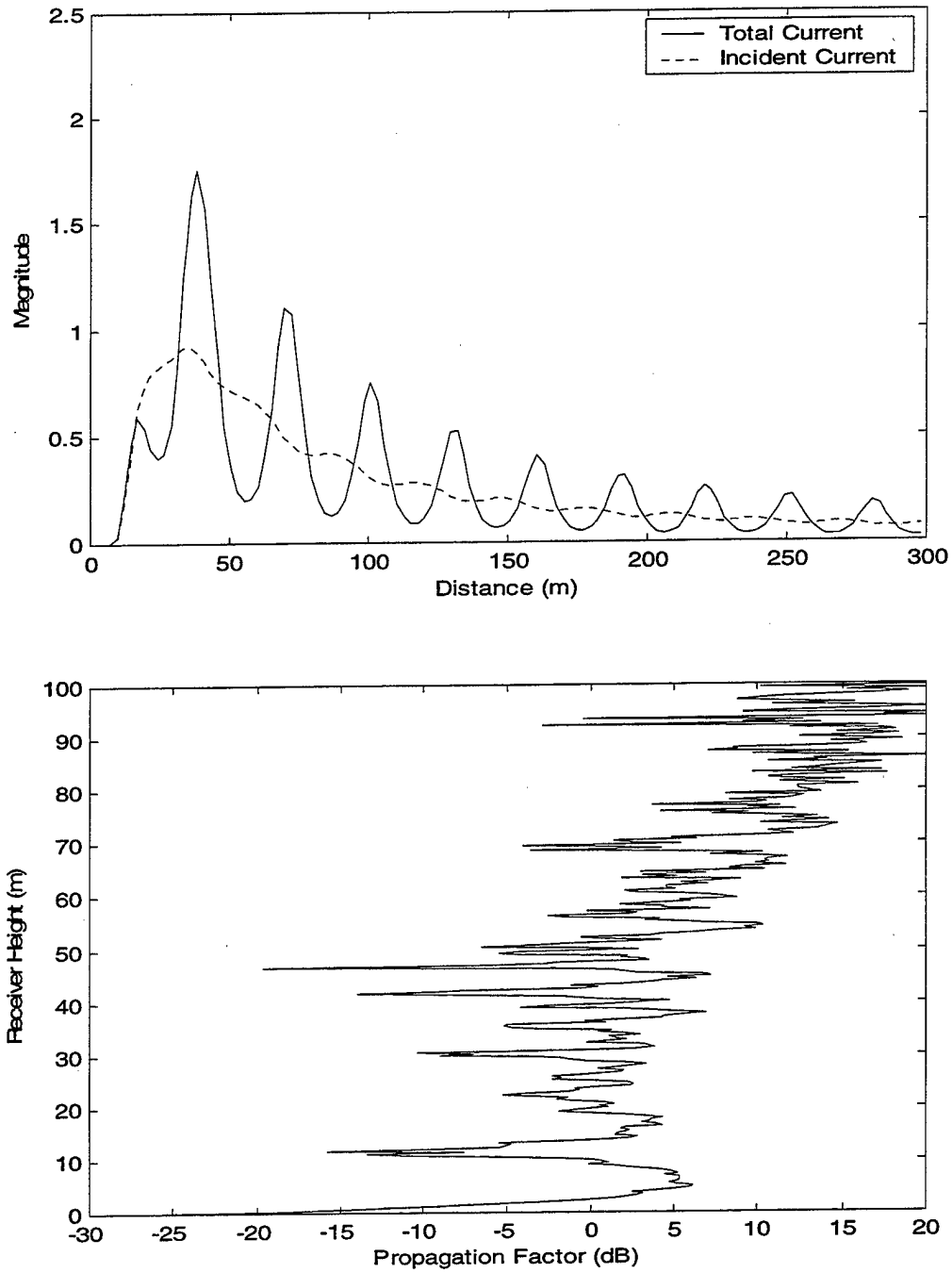

Figure 35: Total Current and Incident Current (Upper Figure) and Propagation Factor (Lower Figure) for Propagation over Sinusoidal Surface. $\Delta_x = 8\lambda$, $\sigma_z = \frac{4\lambda}{3}$

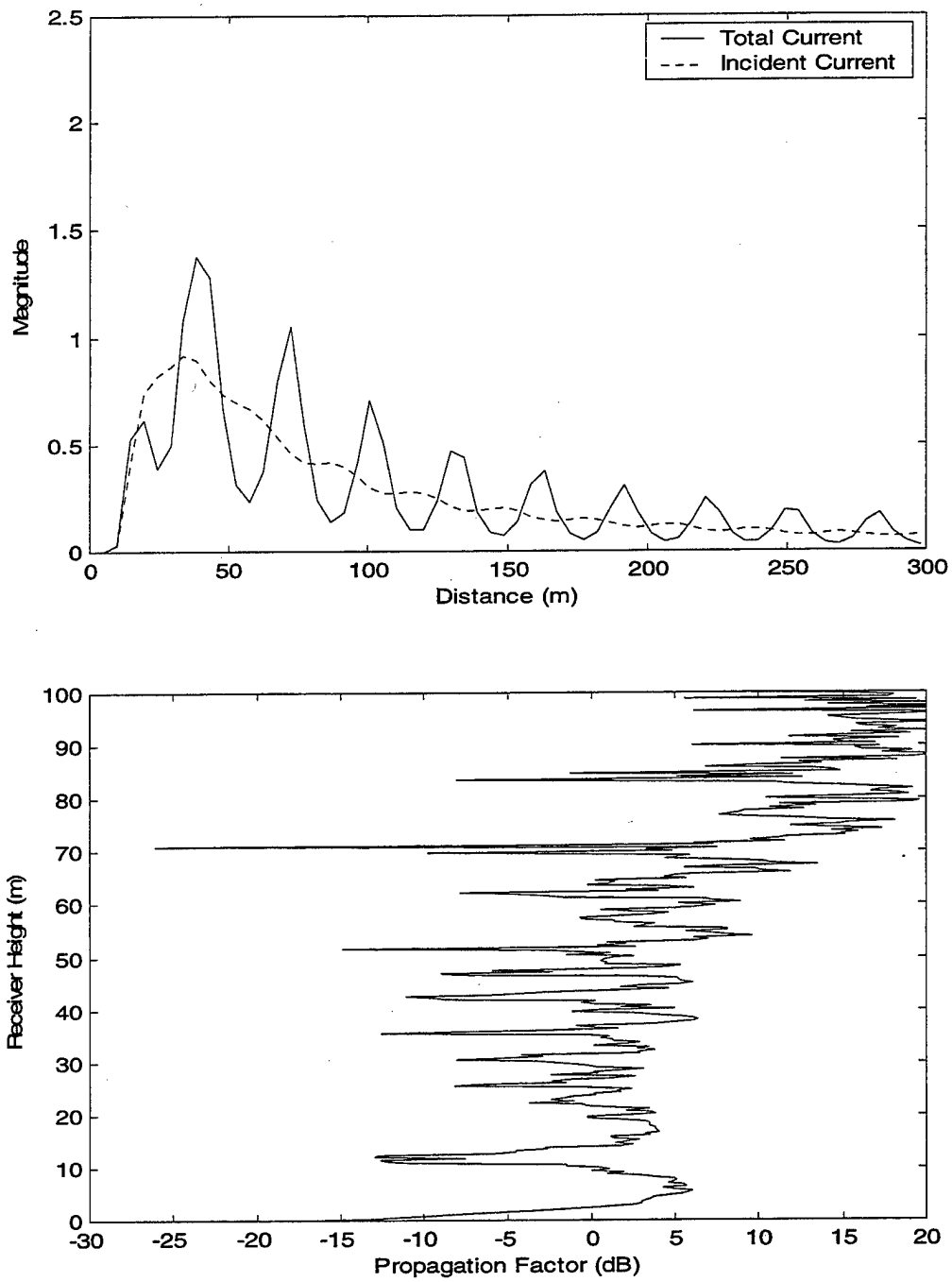

Figure 36: Total Current and Incident Current (Upper Figure) and Propagation Factor (Lower Figure) for Propagation over Sinusoidal Surface. $\Delta_x = 16\lambda$, $\sigma_z = \frac{4\lambda}{3}$

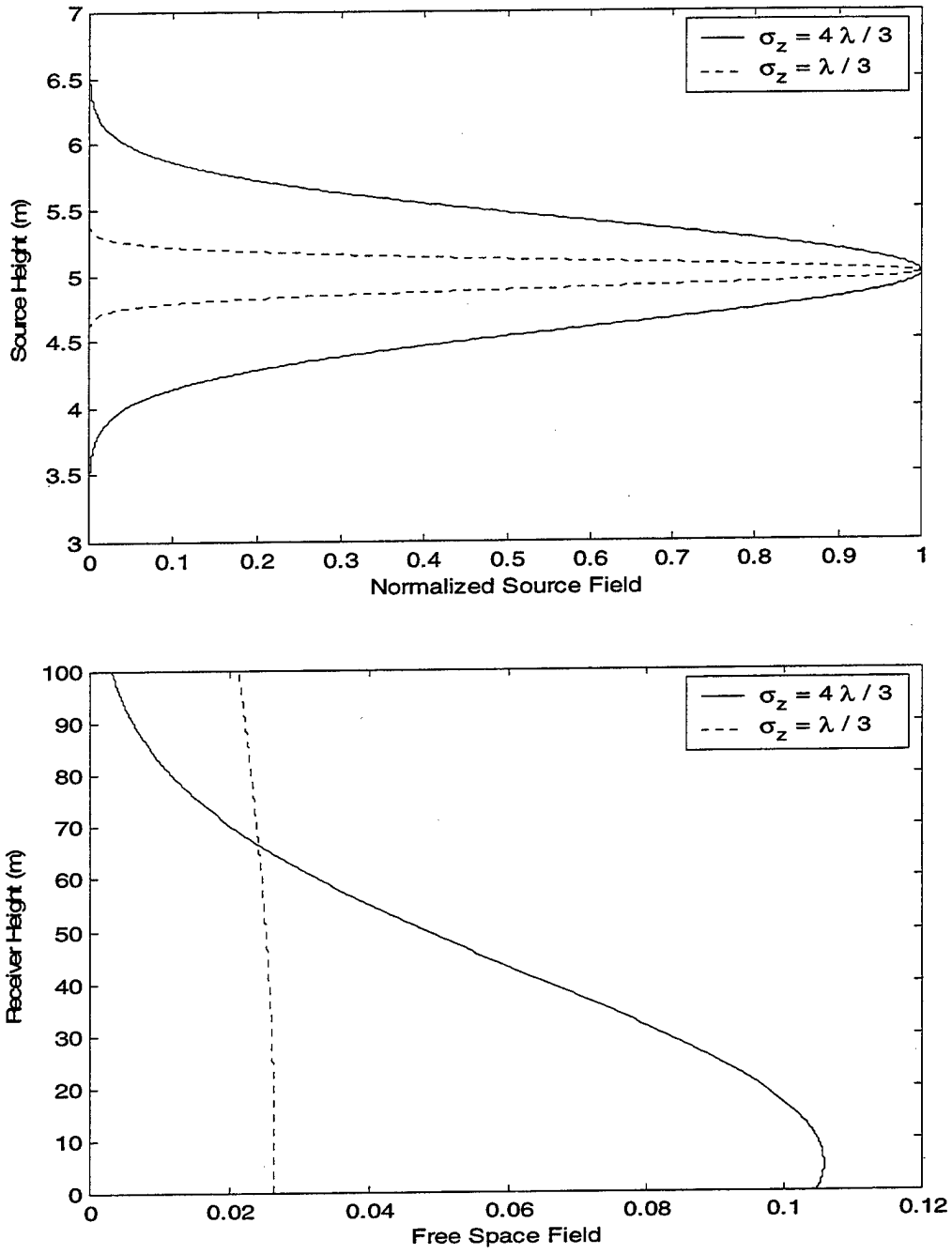

Figure 37: Normalized Source Field (Upper Figure) and Free Space Field (Lower Figure) at $x = 300$ m. Transmitter Antenna Height = 5 m. Frequency = 1 GHz

3. Equivalent Impedance Determination

Once we have calculated the propagation factor for the sinusoidal surface, we can find the equivalent impedance of the sinusoidal surface for low grazing angles. If we compare Figure 7 and Figure 19 we notice that for small receiver heights (= low grazing angles) both curves have approximately the same shape. This can give us an intuitive explanation that under these circumstances we can represent the PEC sinusoidal surface by the lossy flat surface.

Figure 38 shows the real part and the imaginary part of the normalized equivalent impedance $\frac{1}{\sqrt{\epsilon_{rc}}}$ for the sinusoidal surface using the following parameters: $z_t = 1.5\,\text{m}$, $A_{pp} = 1\,\text{m}$, $T = 30\,\text{m}$ and $x = 300\,\text{m}$. We ran the problem 50 times with θ uniformly distributed in the interval $[0,2\pi]$. We can see that as the grazing angle approaches zero, the real part tends to 1.69 and the imaginary part tends to 4.58. Notice the dashed line in the first plot on Figure 38, which represents the best linear fit when minimizing the sum of the squared error. If we now run the flat surface problem with these values we obtain the same results for PF as the sinusoidal surface when averaged over many realizations. Notice the bottom plot on Figure 38. Figure 39 shows results when running 100 realizations. We notice that as the grazing angle approaches zero, the real part tends to 2.16 and the imaginary part tends to 4.56.

In Figure 40 we ran 50 realizations with the parameters described above ($z_t = 1.5\,\text{m}$, $A_{pp} = 1\,\text{m}$, $T = 30\,\text{m}$, $x = 300\,\text{m}$ and θ uniformly distributed in the interval $[0,2\pi]$), but we changed the maximum receiver height to 78 m, or, equivalently, the maximum grazing angle to 15°. Then, using the equivalent impedance found when

performing the fitting for low grazing angles (real part tending to 1.69 and imaginary part tending to 4.58) we calculated the equivalent PF for propagation over flat lossy surface. In the upper figure we notice a linear behavior for both the real and imaginary part of the equivalent impedance for a maximum grazing angle of approximately 7°. In the lower figure we notice a good agreement between the propagation factor when performing 50 realizations and the equivalent flat lossy surface for a maximum height of approximately 15 m. This result is expected, since as we observed in Figure 7 and Figure 19, we have approximately the same shape only for small receiver heights. In other words, the substitution of the sinusoidal PEC surface for a lossy flat surface, when comparing the PF, is valid only for low grazing angles.

For extremely small grazing angles, the errors in $\frac{u}{u_0}$ are amplified by Equation 2.39, due to the presence of $\frac{1}{\sin\psi}$. This is the cause of the large swings in Figure 38, Figure 39, and Figure 40 (upper figures) at low grazing angles and is also the cause of discrepancy seen in the PF in the PF in Figure 38, Figure 39, and Figure 40 (lower figures). Notice that we have smaller swings for one hundred realizations than fifty realizations.

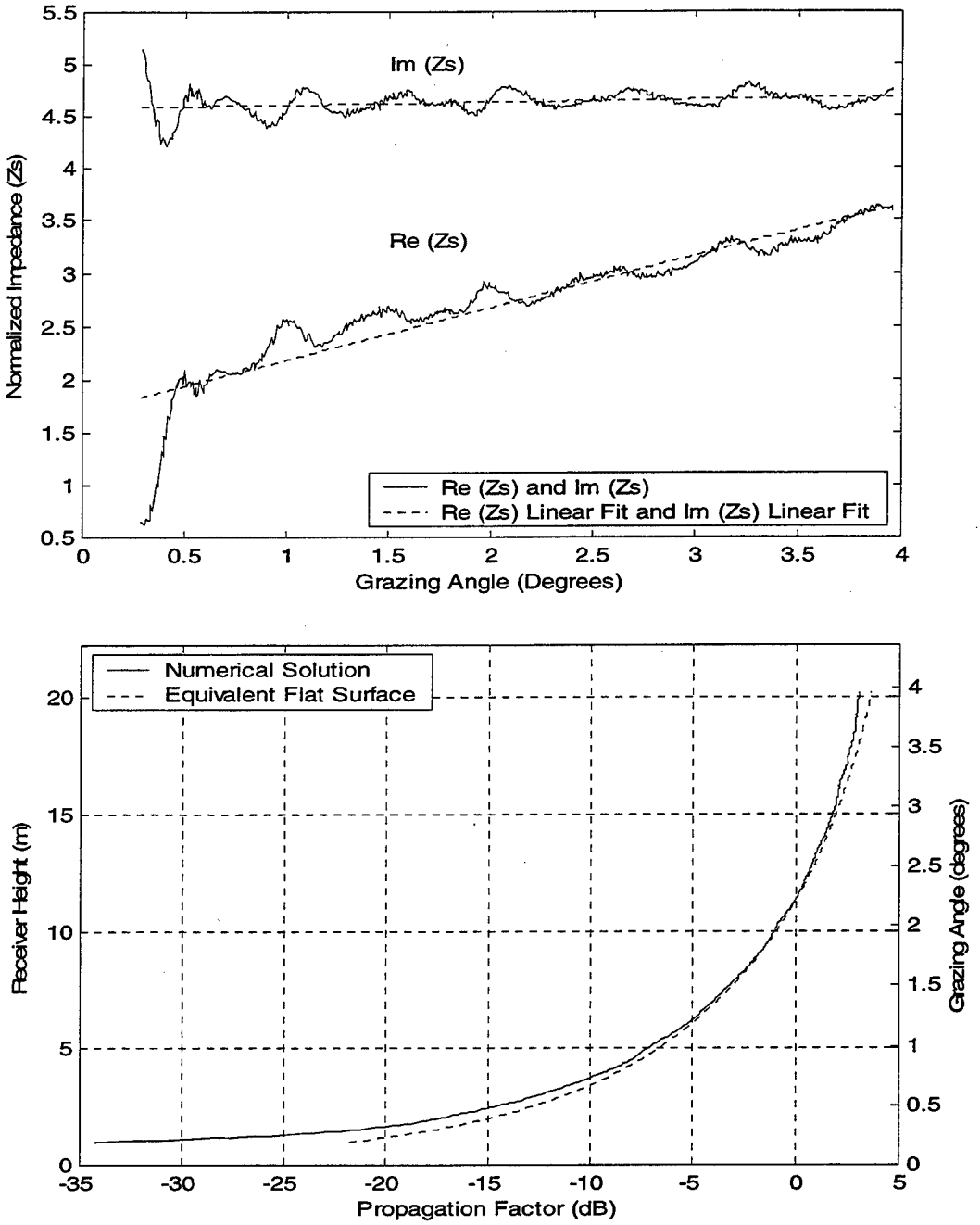

Figure 38: Upper Figure: Equivalent Impedance of Sinusoidal Surface with Period = 30 m and Peak to Peak Amplitude = 1 m. Total Distance = 300 m. Frequency = 1 GHz. Antenna Height = 1.5 m. Δx = 0.3m. Fifty realizations. Lower Figure: PF for the PEC Sinusoidal Surface Above and for the Equivalent Flat Lossy Surface.

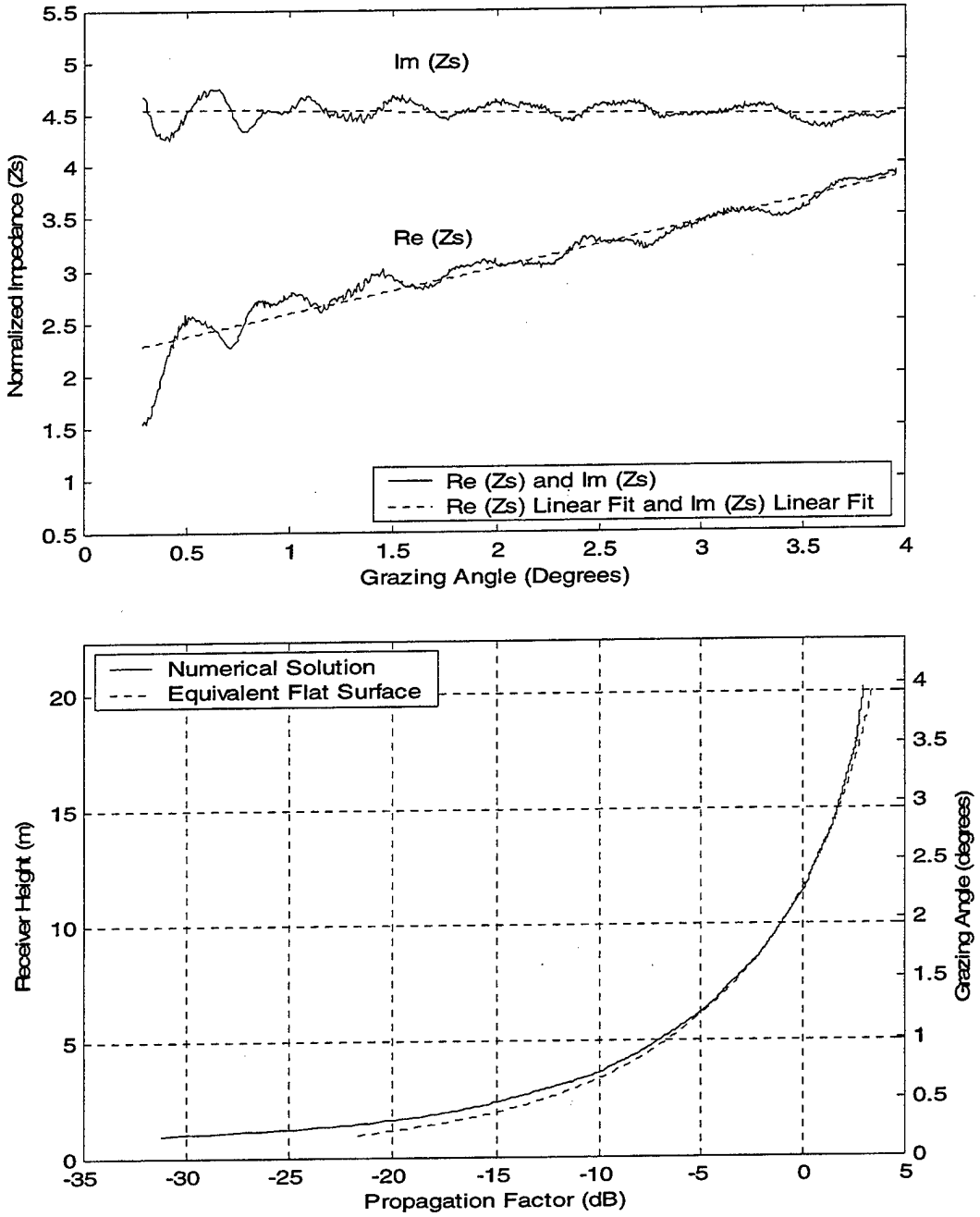

Figure 39: Upper Figure: Equivalent Impedance of Sinusoidal Surface with Period = 30 m and Peak to Peak Amplitude = 1 m. Total Distance = 300 m. Frequency = 1 GHz. Antenna Height = 1.5 m. Δx = 0.3m. One hundred realizations. Lower Figure: PF for the PEC Sinusoidal Surface Above and for the Equivalent Flat Lossy Surface.

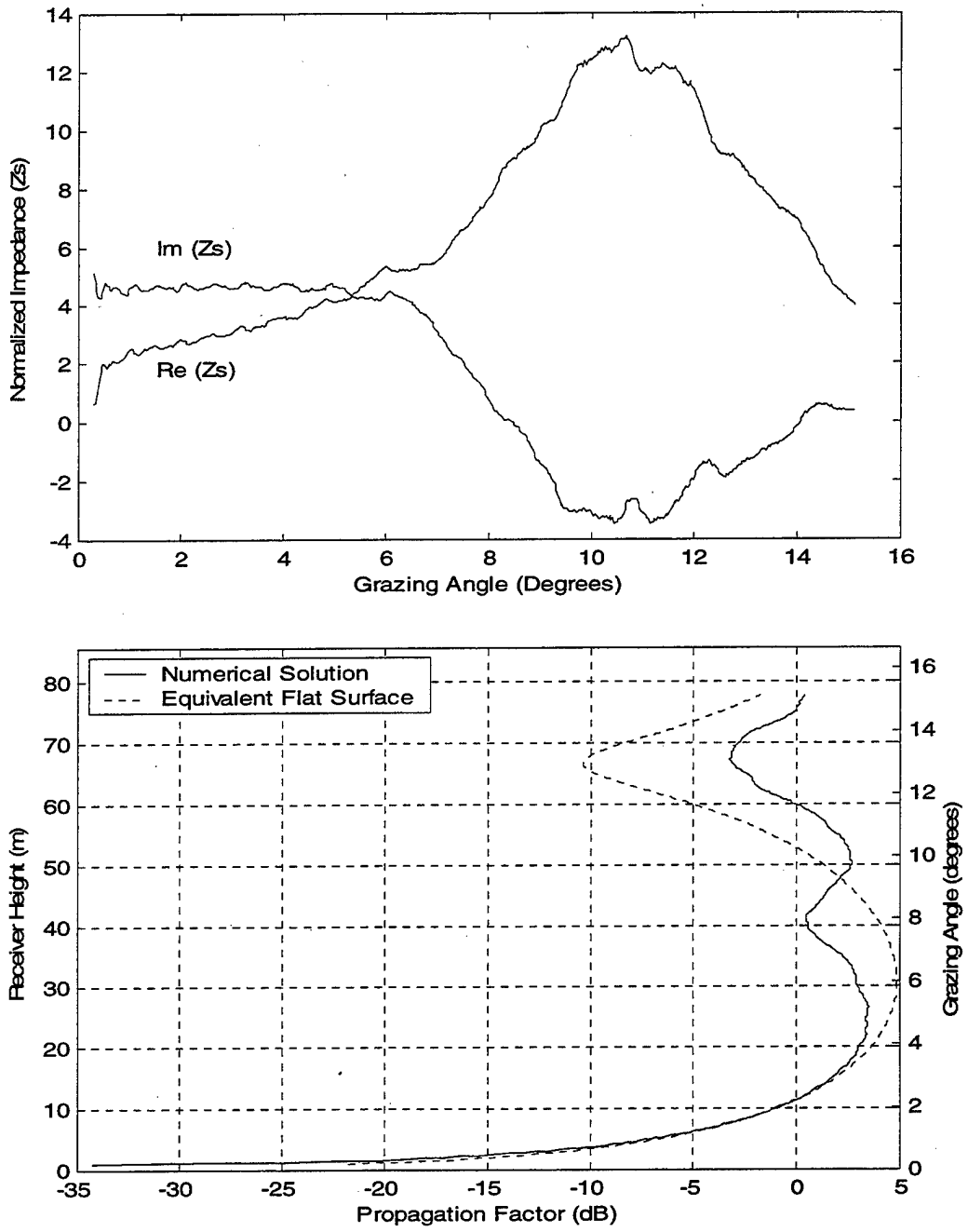

Figure 40: Upper Figure: Equivalent Impedance of Sinusoidal Surface with Period = 30 m and Peak to Peak Amplitude = 1 m. Total Distance = 300 m. Frequency = 1 GHz. Antenna Height = 1.5 m. $\Delta x = 0.3$m. Fifty realizations. Lower Figure: PF for the PEC Sinusoidal Surface Above and for the Equivalent Flat Lossy Surface.

THIS PAGE LEFT INTENTIONALLY BLANK

IV. SEA SURFACE GENERATION

The sea spectrum can be modeled in several different ways depending on the parameters that one tries to represent. In this chapter we will use the *Pierson-Moskowitz spectrum*, which represents the sea spectrum as a function of the wind speed and is given by [Ref. 5]:

$$W(k)=\frac{\alpha}{4|k|^3}e^{-\left(\frac{\beta g^2}{k^2U^4}\right)} \tag{4.1}$$

where $\alpha=8.1\times10^{-3}$, $\beta=0.74$, $g=9.81\ \mathrm{m/s^2}$, $U=$wind speed (m/s) at a height of 19.5 m, $k=\frac{2\pi}{\Lambda}$ is the wave number and Λ is the surface wavelength.

Figure 41 shows the spectrum for wind speed of 5m/s and 6m/s.

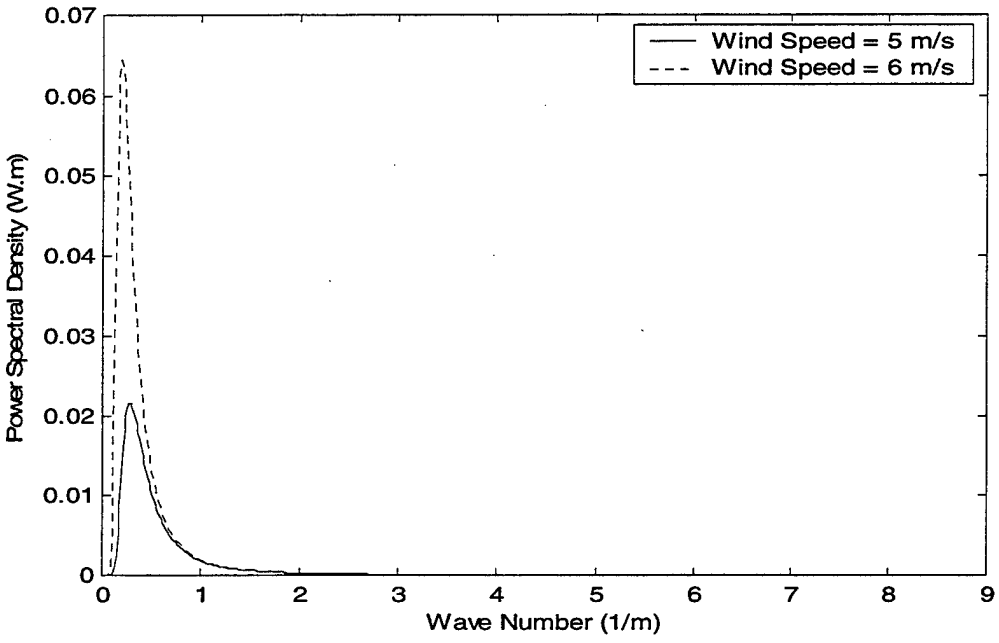

Figure 41: *Pierson-Moskowitz Spectrum* for Wind Speed of 5m/s and 6m/s

Realizations of the random surface will be generated at points $x_n = n\Delta x$ $(n = 1,..., N)$ according to [Ref. 6]:

$$f(x_n) = \frac{1}{L} \sum_{j=-N/2}^{N/2} F(K_j) e^{iK_j x_n}, \tag{4.2}$$

where, for $j \geq 0$,

$$F(K_j) = \sqrt{2\pi L W(K_j)} \begin{cases} \dfrac{[N(0,1) + iN(0,1)]}{\sqrt{2}}, & j \neq 0, \dfrac{N}{2} \\ N(0,1), & j = 0, \dfrac{N}{2} \end{cases} \tag{4.3}$$

and, for $j < 0$, $F(K_j) = F^*(K_j)$. In Equation 4.3 $K_j = \dfrac{2\pi j}{L}$, where L is the surface length and each time $N(0,1)$ appears it represents an independent sample taken from a zero mean, unit variance Gaussian distribution. Equation 4.2 is computed with a fast Fourier transform.

Figure 42 (upper figure) shows a possible surface realization for a wind speed of $5\,\text{m/s}$. Since the parabolic equation has a limited angular response [Ref. 2] we can avoid high slopes smoothing the surface, i.e., changing a local point by the average between itself and some neighbors points. Figure 42 (lower figure) shows the realization of the upper figure when replacing any point by the moving average of itself and four neighbors, two to the right and two to the left. When making use of this smoothing process we practically do not change the statistics of the surface. Figure 43 (upper figure) shows a comparison between the inverse Fourier transform of the noisy spectrum and the autocorrelation of the rough surface for the wind speed of $5\,\text{m/s}$. Figure 43

(lower figure) shows the same comparison, but replacing the autocorrelation of the rough surface by the autocorrelation of the smoothed rough surface.

Defining the *correlation length* 'l' as the length such that $0.5 \times l$ equals the area under the autocorrelation function (only for positive lags) and d_x as the separation between two consecutive points on the rough surface, we need to have

$$L >> l \text{ and } l >> d_x$$

in order to have a truly uncorrelated surface. In the example above, where we had the wind speed of $5\,\text{m/s}$, we had $L = 300\,\text{m}$, $l = 21.2\,\text{m}$ and $d_x = 0.29\,\text{m}$.

Figure 44 shows a surface realization (top figure) and the respectively smoothed surface realization (bottom figure) for a wind speed of $20\,\text{m/s}$. Notice that the surface heights increase substantially when compared to Figure 42. Figure 45 (upper figure) shows a comparison between the inverse Fourier transform of the noisy spectrum and the autocorrelation of the rough surface for the wind speed of $20\,\text{m/s}$. Figure 45 (lower figure) shows the same comparison, but replacing the autocorrelation of the rough surface by the autocorrelation of the smoothed rough surface. For this case we of wind speed of $20\,\text{m/s}$ we have $L = 2000\,\text{m}$, $l = 469.9\,\text{m}$ and $d_x = 3.9\,\text{m}$.

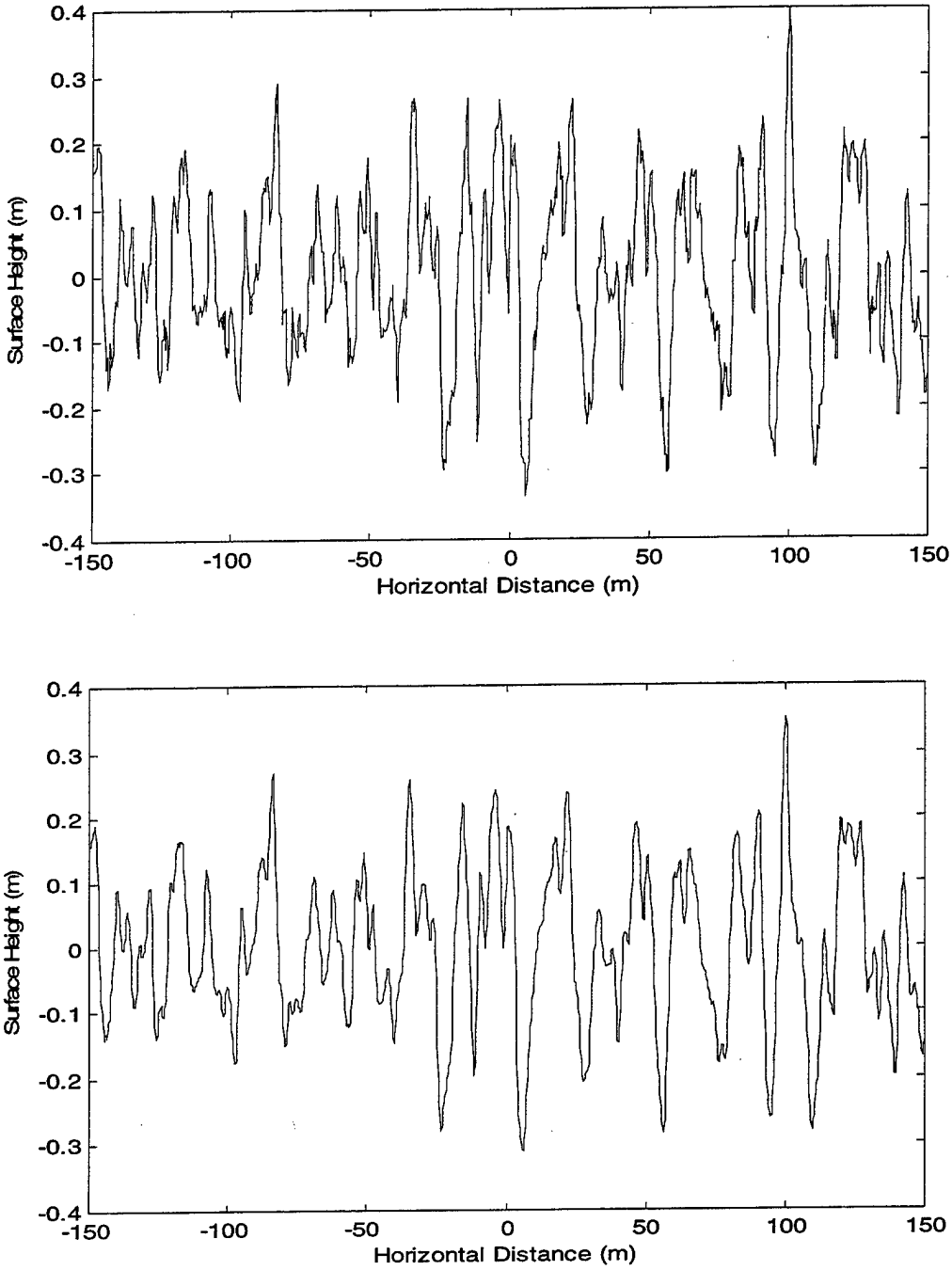

Figure 42: Sea Surface Realization for Wind Speed of 5m/s (Upper Figure) and Smoothed Sea Surface (Averaging Five Points) for Wind Speed of 5m/s (Lower Figure). Length = 300m

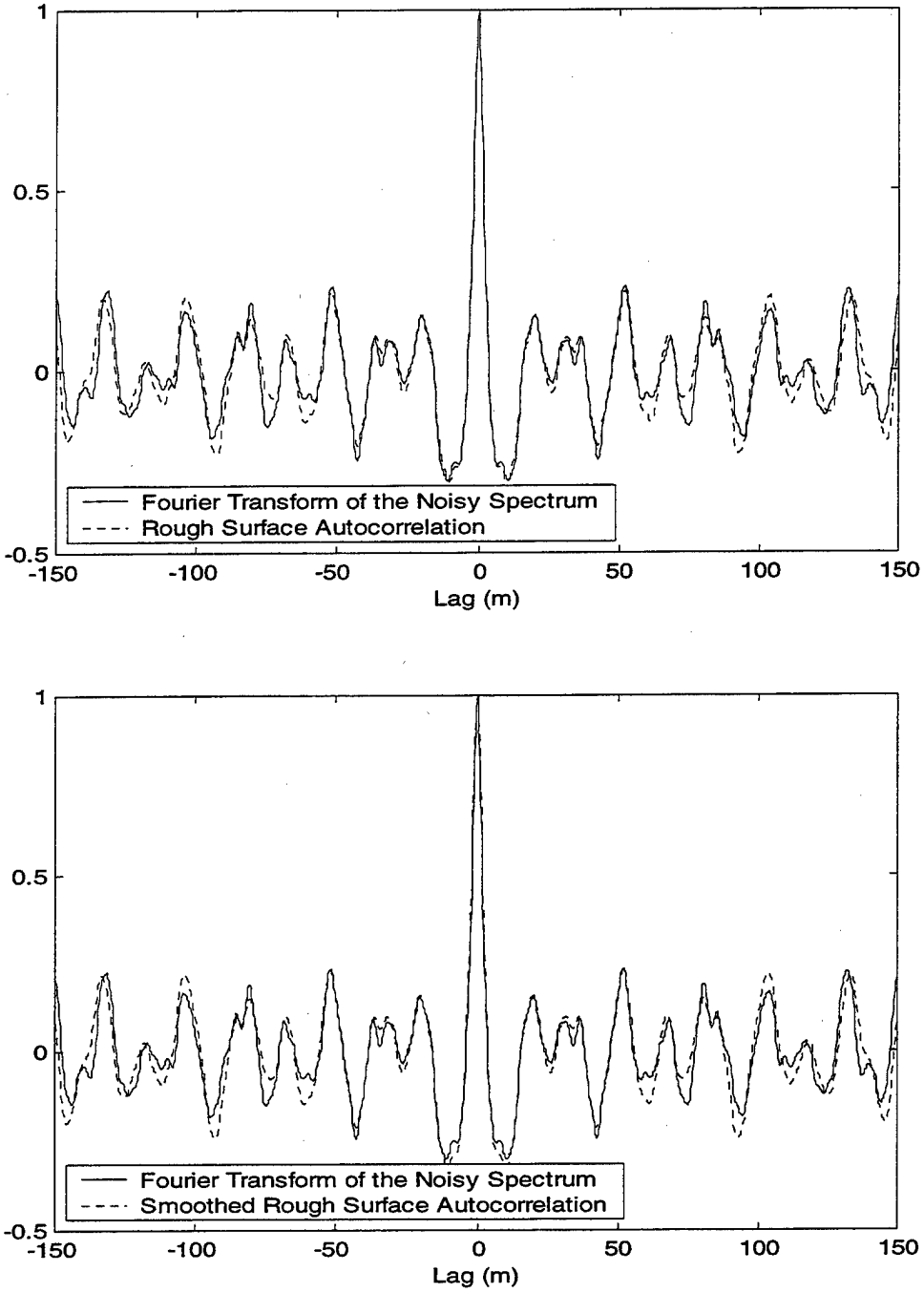

Figure 43: Normalized Fourier Transform of the Noisy Spectrum and Rough Surface Autocorrelation (Upper Figure) and Normalized Fourier Transform of the Noisy Spectrum and Smoothed Rough Surface Autocorrelation (Lower Figure). Wind Speed = 5m/s

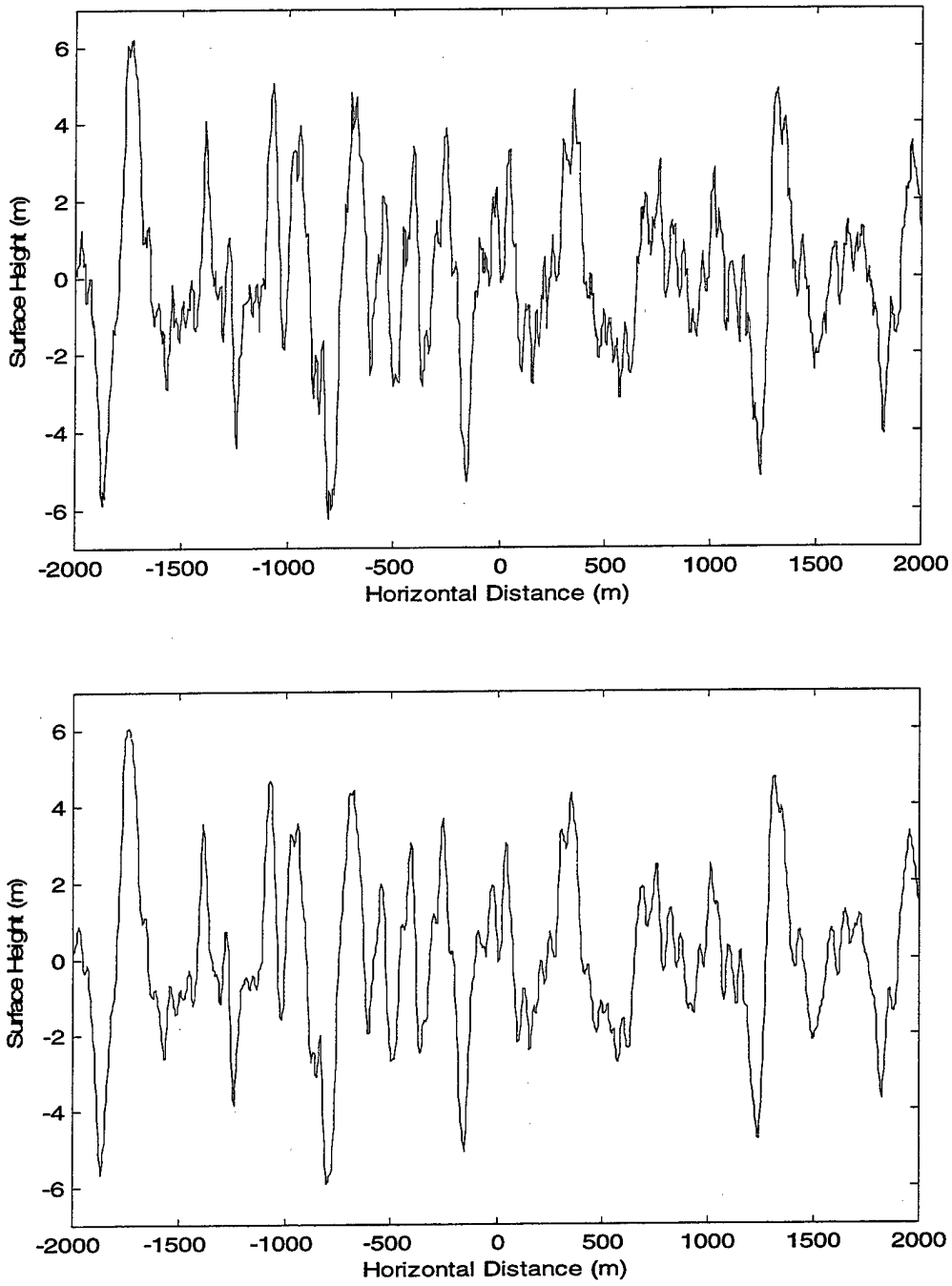

Figure 44: Sea Surface Realization for Wind Speed of 20m/s (Upper Figure) and Smoothed Sea Surface (Averaging Five Points) for Wind Speed of 20m/s (Lower Figure). Length = 4000m

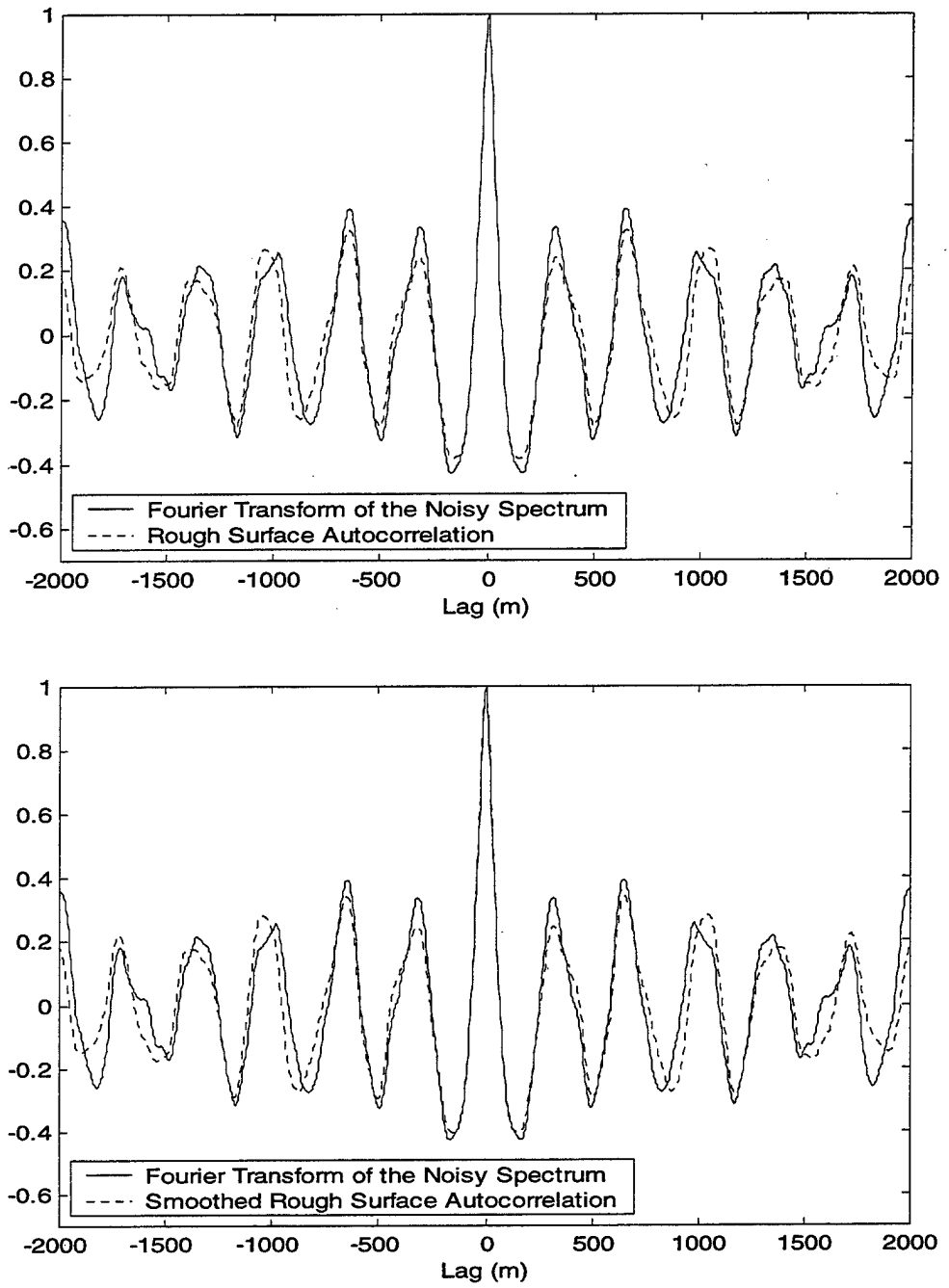

Figure 45: Normalized Fourier Transform of the Noisy Spectrum and Rough Surface Autocorrelation (Upper Figure) and Normalized Fourier Transform of the Noisy Spectrum and Smoothed Rough Surface Autocorrelation (Lower Figure). Wind Speed = 20m/s

THIS PAGE LEFT INTENTIONALLY BLANK

V. CONCLUSIONS AND RECOMMENDATIONS

In this thesis, a numerical method to model propagation over random rough surface using the parabolic equation was implemented and tested. The parabolic equation, where the Helmholtz equation is approximated by a parabolic equation, is a quasi-full wave method and takes into account aspects such as forward reflection, diffraction, refraction and surface wave propagation. However, it ignores back-scattering. Because of this assumption, it is possible to use a marching scheme, where the field at a certain point is calculated uniquely based on the field at a previous point, resulting in a very efficient computational method. Besides, this method seems to be the only practical method for predicting radiowave propagation over long ranges (thousands of wavelengths) and over a wideband of frequencies.

Since our technique uses a Volterra integral equation of the second kind, the numerical computations become very intense for large distances. In order to minimize the computation time, we introduced a multiple sections solution, where the numerical solution scheme is successively repeated for smaller ranges. Given the field on a vertical line between two sections we calculate the current on the surface between these two vertical lines and then calculate the field on the next vertical line. When using this multiple sections solution we substantially decrease the computation time, although we noticed that when sections become too small numerical errors were introduced.

We tested our numerical techniques for some test cases encountered in the literature such as propagation over a PEC flat surface and over an ideal absorbing knife-edge. The agreement between the numerical solution and these test cases was good.

Next we tested our numerical solution for propagation over a sinusoidal surface. We noticed that for low grazing angles the propagation factor has a shape similar to the one when propagation takes place over a flat lossy surface. This fact served as motivation for modeling the difficult problem of propagation over a rough surface at low grazing angles by propagation over an equivalent impedance plane. We simulated a random surface with a fixed spectrum by translating the sinusoidal surface of given peak to peak height and period in a random fashion, with a uniform distribution in $[0,2\pi]$. Then we compared the resulting normalized field to the field of a 2-ray model over a constant impedance plane. For low grazing angles the agreement was excellent. Finally we showed how to generate rough sea surfaces according to the *Pierson-Moskowitz spectrum*, which represents the sea spectrum as a function of the wind speed.

This thesis represents an effort to predict radiowave propagation over a random rough surface such as the sea. The next step should be to predict the propagation factor for propagation over the sea surface. Finally, because the solution of the Volterra integral equation takes significant amount of CPU time during recursions, the source code should be implemented in a programming language that deals with *for* loops efficiently, such as *C* or *FORTRAN*. In this thesis we used *MATLAB*, which is known to be very efficient for matrix manipulation, but very inefficient for loops.

LIST OF REFERENCES

1. Janaswamy, R., Unpublished Notes, Naval Postgraduate School, Monterey, CA.
2. Jensen, F.B., Kuperman, W.A., Porter, M.B. and Schmidt, H., *Computational Ocean Acoustics*, American Institute of Physics, New York.
3. Abramowitz, M. and Stegun, A., *Handbook of Mathematical Functions with Formulas, Graphs and Mathematical Tables*, Dover Publications, Inc., New York, 1964.
4. Anderson, L.J. and Trolese, L.G., "Simplified Method for computing Knife Edge Diffraction in the Shadow Region," *IRE Transactions on Antennas and Propagation*, pp. 281-286, July 1958.
5. Thorsos, E. I., "Acoustic Scattering from a Pierson-Moskowitz Sea Surface," *Journal of Acoustic Society of America 88* (1), January 1990.
6. Thorsos, E. I., "The Validity of the Kirchhoff Approximation for Rough Surface Scattering Using a Gaussian Roughness Spectrum," *Journal of Acoustic Society of America 83* (1), January 1988.

THIS PAGE LEFT INTENTIONALLY BLANK

INITIAL DISTRIBUTION LIST

No. of Copies

1. Defense Technical Information Center 2
   8725 John J. Kingman Rd., STE 0944
   Ft. Belvoir, Virginia 22060-6218

2. Dudley Knox Library 2
   Naval Postgraduate School
   411 Dyer Rd.
   Monterey, California, 93943-5101

3. Chairman, Code EC 1
   Department of Electrical and Computer Engineering
   Naval Postgraduate School
   Monterey, California, 93943-5121

4. Professor Ramakrishna Janaswamy, Code EC/Js 1
   Department of Electrical and Computer Engineering
   Naval Postgraduate School
   Monterey, California, 93943-5121

5. Professor David Jenn, Code EC/Jn 1
   Department of Electrical and Computer Engineering
   Naval Postgraduate School
   Monterey, California, 93943-5121

6. Professor Kenneth Davidson, Code MR/Ds.....1
   Department of Meteorology
   Naval Postgraduate School
   Monterey, California, 93943-5114

7. Professor Rasler Smith, Code EC/Sr 1
Department of Electrical and Computer Engineering
Naval Postgraduate School
Monterey, California, 93943-5121

8. LCDR Marcelo Jorge de Assis Motta 3
Diretoria de Telecomunicações da Marinha
(Brazilian Navy Telecommunications Directorate)
Rua Primeiro de Março, 118
CEP 20000
Rio de Janeiro – RJ
Brazil

9. Commanding Officer 1
Attention: Herbert Hitney
SPAWARSYSCEN SAN DIEGO
53560 Hull St.
San Diego, CA 92152-5001

10. Commanding Officer 1
Attention: Amalia Barrios
SPAWARSYSCEN SAN DIEGO
53560 Hull St.
San Diego, CA 92152-5001

11. Commanding Officer 1
Attention: Richard Paulus
SPAWARSYSCEN SAN DIEGO
53560 Hull St.
San Diego, CA 92152-5001